Accepted Manuscript W6709.

Rare Earth Element Abundances in Hydrothermal Fluids from the Manus Basin, Papua New Guinea: Indicators of Sub-seafloor Hydrothermal Processes in Back-Arc Basins

Paul R. Craddock[a,1*], Wolfgang Bach[b], Jeffrey S. Seewald[a], Olivier J. Rouxel[a,c], Eoghan Reeves[a] and Margaret K. Tivey[a]

[a] *Department of Marine Chemistry and Geochemistry, Woods Hole Oceanographic Institution, 360 Woods Hole Road, Woods Hole, MA 02543, USA.*

[b] *University of Bremen, Geosciences Department, Klagenfurter Straße, 28359 Bremen, Germany.*

[c] *Université Européene de Bretagne, Institut Universitaire Européen de la Mer, 29280 Plouzané, France.*

[1] *Present address: Origins Laboratory, Department of Geophysical Sciences, University of Chicago, 5734 South Ellis Avenue, Chicago, IL 60637, USA.*

** Corresponding author. Email: craddock@uchicago.edu, Tel: (773) 834 3997*

Submitted to Geochimica et Cosmochimica Acta, July 3, 2009.

Submitted in revised format, May 2, 2010.

ABSTRACT

Rare earth element (REE) concentrations are reported for a large suite of seafloor vent fluids from four hydrothermal systems in the Manus back–arc basin (Vienna Woods, PACMANUS, DESMOS and SuSu Knolls vent areas). Sampled vent fluids show a wide range of absolute REE concentrations and chondrite–normalized (REE_N) distribution patterns (La_N/Sm_N ~ 0.6 – 11; La_N/Yb_N ~ 0.6 – 71; Eu_N/Eu^*_N ~ 1 – 55). REE_N distribution patterns in different vent fluids range from light–REE enriched, to mid– and heavy–REE enriched, to flat, and have a range of positive Eu–anomalies. This heterogeneity contrasts markedly with relatively uniform REE_N distribution patterns of mid–ocean ridge hydrothermal fluids. In Manus Basin fluids, aqueous REE compositions do not inherit directly or show a clear relationship with the REE compositions of primary crustal rocks with which hydrothermal fluids interact. These results suggest that the REEs are less sensitive indicators of primary crustal rock composition despite crustal rocks being the dominant source of REEs in submarine hydrothermal fluids. In contrast, differences in aqueous REE compositions are consistently correlated with differences in fluid pH and ligand (chloride, fluoride and sulfate) concentrations. Our results suggest that the REEs can be used as an indicator of the type of magmatic acid volatile (i.e., presence of HF, SO_2) degassing in submarine hydrothermal systems. Additional fluid data suggest that near seafloor mixing between high–temperature hydrothermal fluid and locally entrained seawater at many vent areas in the Manus Basin causes anhydrite precipitation. Anhydrite effectively incorporates REE and likely affects measured fluid REE concentrations, but does not affect their relative distributions.

1. INTRODUCTION

Rare earth element (REE) distributions in submarine hydrothermal fluids have been used extensively as a tracer of sub–seafloor processes associated with hydrothermal activity including crustal (i.e., aluminosilicate) alteration by high-temperature hydrothermal fluids. Studies of REEs in seafloor vent fluids have focused mostly on basalt–hosted hydrothermal systems along mid–ocean ridge (MOR) spreading centers where fluids have remarkably uniform chondrite–normalized REE (REE_N) distribution patterns characterized by a light REE enrichment and large, positive Eu anomaly (Michard et al., 1983; Michard and Albarede, 1986; Michard, 1989; Klinkhammer et al., 1994b; Mitra et al., 1994; Bau and Dulski, 1999; Douville et al., 1999). REE enrichments in seafloor hydrothermal fluids relative to ambient seawater reflect removal from crustal rock during fluid–rock reaction. It has been suggested that plagioclase dissolution controls the distribution of REEs in submarine hydrothermal fluids because the chondrite–normalized REE (REE_N) compositions of MOR hydrothermal fluids and plagioclase are similar (Campbell et al., 1988b; Klinkhammer et al., 1994b). Laboratory studies, however, suggest that REE compositions of seafloor vent fluids are unrelated to primary rock composition because REE_N distribution patterns in experimental hydrothermal solutions are different from primary REE_N compositions of the volcanic rock or individual minerals with which these fluids have reacted (Bach and Irber, 1998; Möller, 2002; Allen and Seyfried, 2005). These studies suggest that vent fluid REE compositions reflect solubility control during fluid–rock interaction influenced by aqueous REE speciation (c.f., Bau, 1991), which in turn is strongly influenced by numerous aspects of fluid chemistry such as pH, temperature and the availability of ligands. Collectively, these factors lead to fractionation of REEs in sub–seafloor environments.

This study reports REE data for 36 seafloor vent fluids from four active hydrothermal systems (Vienna Woods, PACMANUS, DESMOS and SuSu Knolls) in the Manus back-arc basin, Papua New Guinea. Prior to this study, limited data existed for REE compositions of vent fluids and deposits (e.g., anhydrite) recovered from the Manus Basin or other back-arc basins (e.g., Douville et al., 1999; Bach et al., 2003). Bach et al. (2003) proposed that the heterogeneous REE_N patterns recorded by anhydrite recovered from PACMANUS reflected differences in aqueous REE concentrations that are associated with changes in fluid composition (Cl^-, F^- and SO_4^{2-} ligand concentrations) owing to varying inputs of magmatic volatiles (H_2O–CO_2–SO_2–HCl–HF). The Manus Basin is an ideal area to investigate factors that govern the aqueous abundance of REEs because the composition of underlying crustal rocks differs significantly among vent fields, ranging from basalt to rhyolite (Sinton et al., 2003; Bach et al., 2007; Sun et al., 2007). In addition, vent fluid composition (e.g., pH and ligand concentrations) and temperature differ substantially between fields owing to varying degrees of magmatic volatile degassing either on-going or in the recent past (Seewald et al., 2006; Reeves, 2010). Our data are used to examine the relationship between measured aqueous REE concentrations and host rock compositions to assess whether aqueous REE abundances are controlled primarily by crustal rock composition or aspects of fluid chemistry that affect REE solubility during sub–seafloor fluid–rock interaction. Following on from the study of Bach et al. (2003), our data are also used to examine the sensitivity of aqueous REE abundances to different fluid compositions owing to varying styles of magmatic acid volatile input. The present study provides a better understanding of how measured REE abundances in seafloor vent fluids can be used as tracers of sub–seafloor processes affecting the formation of submarine hydrothermal fluids.

2. GEOLOGIC SETTING

The Manus Basin in the Bismarck Sea, Papua New Guinea (Fig. 1) is a rapidly–opening (~ 100 mm/yr) back–arc basin associated with subduction of the Solomon Microplate beneath the New Britain arc (Taylor, 1979; Davies et al., 1987; Martinez and Taylor, 1996). Crustal extension and spreading are complex and variable and occur along several distinct lineations. Toward the west is the Manus Spreading Center (MSC) bounded between the Willaumez and Djaul transform faults (Martinez and Taylor, 1996). Lavas erupted at the MSC are dominantly basaltic in composition (Both et al., 1986; Sinton et al., 2003; Bach et al., 2007). Several areas of hydrothermal activity have been identified in the MSC; Vienna Woods is the largest and most active of the known fields (Tufar, 1990; Tivey et al., 2007). It is located slightly south of the major spreading center within an axial rift valley at a water depth of ~ 2500 m.

To the east, the Eastern Manus Basin (EMB) is bounded by the Djaul and Weitin transform faults where rapid spreading is accommodated primarily by rifting and extension of existing crust (Martinez and Taylor, 1996). Lavas are erupted as a series of discrete *en echelon* neovolcanic ridges and volcanic cones of felsic (andesite to rhyolite) composition (Sinton et al., 2003; Bach et al., 2007). The arc–affinity of volcanic lavas (Sinton et al., 2003) is consistent with the proximal location (< 200 km) of the EMB to the actively subducting margin. The EMB hosts several known active hydrothermal systems. The Papua New Guinea–Australia–Canada–Manus (PACMANUS) hydrothermal system is located on the crest of the 35 km long, 500 m high Pual Ridge, between water depths of 1650 and 1740 m (Binns and Scott, 1993). The ridge is

91 constructed of several sub–horizontal lava flows with compositions between andesite and dacite
92 (Binns and Scott, 1993; Sinton et al., 2003). There are several discrete vent fields within the
93 PACMANUS system (Fig. 1b) that exhibit varying styles of hydrothermal activity ranging from
94 high–temperature (> 300 °C) black smoker fluid venting from sulfide–rich chimneys to low–
95 temperature diffuse flows through sediment and cracks in lavas. Further to the east, the
96 DESMOS and SuSu Knolls hydrothermal systems are located on individual volcanic structures
97 in environments that are markedly different from the ridge–hosted Vienna Woods and
98 PACMANUS hydrothermal fields. DESMOS (Onsen Field, Sakai et al., 1991; Gamo et al.,
99 1997) is located at the crescent–shaped North wall of a caldera located in a water depth of ~
100 1900 to 2000 m. Basaltic to andesitic pillow flows and hyaloclastite deposits arranged across
101 several terraces form the slopes of the caldera. Sedimentation and alteration of primary lavas is
102 common and includes Fe–oxide staining and acid–sulfate (advanced argillic) alteration, locally
103 abundant native sulfur flows and extensive presumed microbial mats (Sakai et al., 1991; Gamo et
104 al., 1997; Gena et al., 2001). Further east, SuSu Knolls consists of three discrete volcanic cones
105 (Suzette, North Su and South Su; Fig. 1c) at water depths between ~ 1140 and 1510 m (Binns et
106 al., 1997; Tivey et al., 2007). The North Su and South Su volcanic structures are composed of
107 abundant porphyritic dacite flows showing variable acid–sulfate type alteration (i.e., quartz–
108 pyrophyllite–illite–alunite and native sulfur) and sedimentation by mixed volcaniclastic and
109 hydrothermal material (Binns et al., 1997; Yeats et al., 2000; Hrischeva et al., 2007; Tivey et al.,
110 2007). The Suzette volcanic structure is extensively coated in metalliferous sediment and relict
111 sulfide talus that overlies primary and/or secondary volcanic features (Hrischeva et al., 2007;
112 Tivey et al., 2007).
113

2.1. Hydrothermal Activity

2.1.1. Vienna Woods

Current hydrothermal activity is manifest as both focused and diffuse fluid venting within an area of ~ 150 m by 100 m (Tufar, 1990; Tivey et al., 2007). Inactive sulfide chimneys extend across a total area ~ 300 m by 100 m. Mildly acidic (pH (25 °C) 4.2 to 4.7), clear and gray smoker fluids with temperatures between 273 and 283 °C were sampled exiting the tops of large sulfide–rich chimneys up to 7 m in height (Seewald et al., 2006).

2.1.2. PACMANUS

Current hydrothermal activity occurs at several discrete vent fields (Roman Ruins, Roger's Ruins, Satanic Mills, Snowcap, Tsukushi and Fenway) that are each between 50 and 200 m in diameter (Binns et al., 2007; Tivey et al., 2007). Vent fluids with a range of temperature and composition were sampled from these fields, including high temperature fluids (~ 300 – 358 °C) with focused discharge from black smoker chimneys, lower temperature white/gray smoker fluids (150 – 290 °C) discharging from "diffuser" chimneys that lack a central open conduit, and low temperature diffuse fluids (< 100 °C) exiting through cracks in the volcanic basement or metalliferous deposits and sediments. The measured pH (25 °C) of all high temperature vent fluids (> 240 °C) are relatively acidic between 2.3 and 2.8 (Seewald et al., 2006).

2.1.3. DESMOS

Hydrothermal activity occurs at the Onsen field (Gamo et al., 1997), which is a small (~ 30 m diameter) area of moderate temperature fluid discharge located along the northern interior slope of the DESMOS caldera. Seafloor venting is markedly different from high–temperature black smoker fluids and is manifest as thick, milky–white fluids discharging directly through extensively altered volcanic breccia and hydrothermal sediments composed of abundant native sulfur and anhydrite (Gamo et al., 1997; Seewald et al., 2006; Bach et al., 2007). Despite the low temperatures of sampled fluids (< 120 °C), measured pH (25 °C) values are low (< 1.5) and aqueous sulfate abundances exceed that of seawater concentrations (Seewald et al., 2006). On the basis of aqueous compositions, these fluids have been termed 'acid–sulfate' fluids (Gamo et al., 1997).

2.1.4. SuSu Knolls

At SuSu Knolls, hydrothermal activity and vent fluid compositions are remarkably diverse (Seewald et al., 2006). At North Su, the summit of the volcano is dominated by a large sulfide–rich black smoker complex with individual chimneys up to 11 m in height. Vent fluids sampled from this complex are similar to high–temperature black smoker fluids sampled from PACMANUS, with temperatures between 300 and 325 °C and moderate–to–low pH (25 °C) between 2.8 and 3.2 (Seewald et al., 2006). In contrast, the flanks of the volcano are dominated by extensive discharge of acid–sulfate fluids similar to that sampled from DESMOS. Acid–sulfate fluids from North Su have a milky–white color, lower temperatures (48 to 241 °C), are very acidic (pH (25 °C) < 1.8) (Seewald et al., 2006) and exit through cracks in hyaloclastite

flows, extensively altered volcanic breccia and hydrothermal sediments composed of native sulfur and anhydrite (Yeats et al., 2000; Bach et al., 2007; Tivey et al., 2007).

There is currently more limited hydrothermal activity at South Su. This vent field is characterized by outcrops of both fresh and variably altered volcanics overlain by mostly inactive sulfide chimneys and scattered oxide–stained hydrothermal sediments (Yeats et al., 2000; Hrischeva et al., 2007; Tivey et al., 2007). In an area of diffuse venting toward the NW, extensively altered and bleached volcanic rocks were observed (Tivey et al., 2007). High–temperature fluid venting from scattered diffuser–type chimneys was observed and sampled in two areas toward the S and SE. The maximum measured temperature for these fluids was 290 °C. The pH (25 °C) of these fluids is low, ranging from 2.6 to 2.7 (Seewald et al., 2006).

The smaller structure of Suzette, located NW of North Su and South Su, is extensively covered by volcanic breccia, hydrothermal and hemipelagic sediment, mass–wasted sulfide talus, Fe–oxide crusts and limited exposures of possible hydrothermal stockwork (Hrischeva et al., 2007; Tivey et al., 2007). The summit is characterized by large expanses of both relict and scattered active sulfide chimneys that are commonly buried within thick sediment. Hydrothermal activity is intermittent over broad sections of the Suzette mound. Five high–temperature vents, with fluids emanating from sulfide–rich chimney edifices, were sampled. Temperatures ranged from 226 to 303 °C and measured pH (25 °C) from 3.5 to 3.8 (Seewald et al., 2006). A sixth fluid was sampled from a cracked pavement structure; this fluid had a temperature of ~ 249 °C and a considerably lower pH (25 °C) of ~ 2.3 (Seewald et al., 2006).

3. METHODS

3.1. Sample Collection and Processing

A total of 101 hydrothermal fluid samples were collected from 36 vents during *R/V Melville* cruise MGLN06MV (July to September, 2006) using discrete samplers deployed by ROV *Jason II*. Samples were primarily collected in 160 ml isobaric gas–tight samplers (Seewald et al., 2002) and supplemented with fluids collected in 755 ml Ti–syringe or "major" samplers (Von Damm et al., 1985). In most cases, fluids were sampled in triplicate. Temperatures were measured with a thermocouple mounted directly on the snorkel of the isobaric samplers and, in some cases, using the ROV temperature probe. Estimated uncertainty in the measured temperatures is ± 2 °C.

Sample aliquots for chemical analysis were extracted immediately after recovery of the samplers at the end of each dive operation. Fluid samples were drawn into acid cleaned, high–density polyethylene (HDPE) Nalgene^{TM} bottles. Aliquots of fluid drawn for REE and other trace element analysis were immediately acidified to pH < 2 by addition of Fisher Optima^{TM} grade HCl to prevent precipitation of metal sulfides and sulfates from solution during storage prior to on–shore analysis. In nearly all major and gas–tight samplers, a precipitate ("dregs" fraction) formed on the interior walls and bottom of the sampler as the hydrothermal fluid cooled. The dregs were collected on a 0.22 μm pore–size, 45 mm diameter Nylon filter by rinsing with high–purity acetone and Milli–Q water. The Nylon filters were dried and stored in glass vials for on–shore processing. In addition, minor precipitates formed within several acidified aliquots during storage (referred to here as "bottle–filter" fraction). These precipitates were separated from the

206 fluid by filtering through a 0.22 μm Nuclepore® filter as part of shore–based sample processing.
207 The concentrations of REEs in sampled fluids were determined by separate measurement of
208 element concentrations in all dissolved, dregs and bottle-filter fractions followed by
209 mathematical reconstitution of the original fluid. A mass balance for REEs indicates that for
210 fluids analyzed in this study, approximately 90 % of REEs were in the dissolved phase.
211
212 Dissolved fractions were prepared for analysis by gravimetric dilution of a ~ 0.20 g split of each
213 solution using 5% Fisher Optima™ grade HNO_3. Sample dilution factors were adjusted as a
214 function of the chlorinity of the fluid to obtain a uniform 6 mM Cl concentration in all samples.
215 This equated to between 80 and 110 times dilution of the original sample. Dilution to uniform Cl
216 minimized the effect of variable matrix (primarily from Na^+, the major cation in solution) on
217 analyte behavior within the plasma during analysis by inductively coupled plasma–mass
218 spectrometry (ICP–MS). Dregs and bottle–filter fractions were treated separately. Particles were
219 removed from filters into 30 ml Savillex™ vials by rinsing with 5 ml of concentrated Fisher
220 Optima™ HNO_3. The vials were sealed and placed on a hot plate overnight (~ 70 °C) to digest
221 particles. The resulting solutions were then evaporated to dryness. The acid
222 digestion/evaporation step was repeated a further two times to achieve complete dissolution of
223 the sulfide–sulfate mix. The digested particles were redissolved and quantitatively diluted in 5%
224 HNO_3 acid for analysis.
225
226 **3.2. Analytical Methods**
227
228 *3.2.1. Determination of REE concentrations*

Analyses of REE concentrations were performed on a ThermoElectron *Element2* ICP–MS at the Woods Hole Oceanographic Institution. Solutions were introduced into the plasma using a Cetac Aridus® desolvating nebulizer to reduce isobaric interferences (e.g., $^{135}Ba^{16}O^{+}$ on $^{151}Eu^{+}$). Barium– and REE–oxide formation was monitored throughout the analytical session by periodic aspiration of Ba and Ce spikes. Barium–oxide formation was significantly less than 1 %. Significant interference of BaO^{+} on Eu^{+} would bias (decrease) the natural $^{151}Eu/^{153}Eu$ ratio (~ 0.916). In almost all samples no bias was observed and no correction for BaO interference was required. REE–oxide formation was typically less than 1 to 4 % of total REE concentration. Samples were spiked with 1 ppb ^{45}Sc and ^{115}In internal standards to correct for fluctuations of the plasma during the analytical session. Unknown sample concentrations were calibrated against matrix–matched, multi–REE standards prepared from Specpure plasma solution standards. Background intensities were measured periodically by aspirating 5% HNO_3 blanks. External precision, determined by triplicate analysis of randomly selected samples across multiple analytical sessions, was ~10 % (1σ).

3.2.2 Calculation of vent fluid and endmember fluid compositions

Typically, seafloor vent fluid compositions are reported as endmembers assuming that the hydrothermal fluid contains no Mg owing to quantitative Mg uptake during high-temperature fluid-rock interaction (Von Damm, 1983; Von Damm et al., 1985). Nearly all sampled fluids in this study contained measurable Mg. The presence of non-zero Mg reflects either the true non-zero Mg composition of the fluid sampled at the seafloor (e.g., owing to near-seafloor mixing

between seawater and hydrothermal fluid), or artifacts during sampling owing to entrainment of seawater at the sampler snorkel. The measured Mg concentration of fluids sampled in duplicate or triplicate at each discrete vent orifice was typically near identical, which is interpreted as reflecting the true Mg concentration of the fluid exiting the seafloor. Fluids sampled in this study should not be interpreted as being compromised by seawater entrainment during sampling because it is unlikely that identical amounts of seawater (as indicated by the same Mg concentration) would be entrained in two or more independently sampled fluids. REE concentrations for all vent fluids sampled at the seafloor are therefore reported at the lowest measured Mg concentration (Table 1).

REE concentrations in smoker–type fluids are also reported as endmembers (Table 2) by extrapolation of replicate vent fluid compositions to zero Mg using least–squares linear regression forced to pass through the composition of ambient seawater (Von Damm, 1983). The concept of a zero–Mg endmember hydrothermal fluid is useful for understanding the processes occurring in the sub–seafloor (e.g., high–temperature fluid–rock interaction) prior to mixing between hydrothermal fluid and seawater at or close to the seafloor. Calculation of endmember concentrations also allows direct comparison of species compositions among vent fluids examined in this and other studies.

REE concentrations in acid–sulfate fluids sampled from DESMOS and SuSu Knolls (North Su) were not extrapolated to zero–Mg. Our indications are that the concept of a zero–Mg endmember acid–sulfate hydrothermal fluid does not necessarily apply. Acid–sulfate fluids sampled in triplicate contain similar and consistently high Mg concentrations ($\geq$ 24 mmol/kg), but have

elevated temperatures and very low pH. In contrast to typical high-temperature black- and gray-smoker fluids, acid-sulfate fluids appear to absent of convecting seawater-derived hydrothermal fluids that react extensively with fresh crustal rocks and instead appear to have formed primarily by sub–seafloor mixing of a magmatic volatile phase and Mg-rich seawater (Seewald et al., 2006) followed by reaction with extensively altered crustal rocks.

4. RESULTS

4.1. Rare earth element concentrations in Manus Basin hydrothermal fluids

4.1.1. Manus Spreading Center (Vienna Woods)

Total REE concentrations (ΣREE) at Vienna Woods range from ~ 2.6 to 5.8 nmol/kg (Table 1). Chondrite–normalized REE_N distribution patterns are uniformly light–REE (La–Nd) enriched and show a large positive Eu–anomaly (Fig. 2). The data are consistent with REE compositions previously reported for Vienna Woods hydrothermal fluids (Douville et al., 1999). The range of REE concentrations and relative distributions are similar to those measured in high–temperature (≥ 280 °C) vent fluids from basalt–hosted, mid–ocean ridge (MOR) hydrothermal sites (Fig. 2).

4.1.2. Eastern Manus Basin (PACMANUS, DESMOS and SuSu Knolls)

Most hydrothermal fluids sampled from the Eastern Manus Basin have high REE concentrations relative to fluids from Vienna Woods and overall exhibit a broad range of REE_N distribution

298 patterns. Total concentrations of REEs at PACMANUS range from ~ 1.5 to 88 nmol/kg (Table
299 1). The REE_N distribution patterns of most sampled fluids are variably light–REE enriched with
300 a positive Eu anomaly (Fig. 3). Two vent fluids, Satanic Mills (vent SM2) and Fenway (vent F1),
301 have REE_N distribution patterns that show heavy–REE (Dy–Yb) enrichments and positive Eu
302 anomalies (Fig. 3b, c).
303
304 Total REE concentrations in acid–sulfate fluids at DESMOS vary from ~ 147 to 236 nmol/kg
305 (Table 1) and are significantly greater than those of sampled high–temperature black smoker
306 fluids at Vienna Woods and PACMANUS (see also Douville et al., 1999), but are similar to
307 those measured in acid–sulfate fluids from continental geothermal environments (e.g., Valles
308 Caldera, New Mexico (Michard, 1989); Rotokawa and Waiotapu, New Zealand (Wood, 2001)).
309 Chondrite–normalized REE_N distribution patterns are generally flat with a only slight convex–
310 upward curvature and do not have a clear positive or negative Eu anomaly (Fig. 4a). The flat
311 REE_N distributions patterns differ markedly from those of black and gray smoker fluids venting
312 from chimney edifices at other vent fields.
313
314 Total REE concentrations and REE_N distribution patterns show a high degree of variability in
315 vent fluids at SuSu Knolls (Fig. 4). Total REE concentrations in acid–sulfate fluids sampled from
316 North Su range from ~ 93 to 350 nmol/kg (Table 2) and exhibit REE_N distribution patterns that
317 are flat with no clear Eu anomaly (Fig. 4a), similar to REE_N distribution patterns in acid–sulfate
318 fluids at DESMOS. Total concentrations of REEs in smoker fluids from North Su, South Su and
319 Suzette range from ~ 6.5 to 43 nmol/kg. The REE_N distribution patterns of most black/gray
320 smoker fluids are light–REE enriched with pronounced positive Eu anomalies (Fig. 4b–d). Some

smoker fluids sampled from Suzette (vent SZ5) and South Su (vent SS1) have REE_N distribution patterns that exhibit greater enrichment of heavy REEs and smaller Eu anomalies relative to other smoker fluids sampled from the same vent field (Fig. 4b, d).

5. DISCUSSION

5.1. Controls on Aqueous REE Compositions of Seafloor Hydrothermal Fluids

Although there is consensus that the rare earth elements (REEs) in submarine hydrothermal fluids are derived principally from the oceanic crust during high temperature fluid–rock interaction, the primary processes that control the observed chondrite–normalized REE distribution patterns of seafloor vent fluids are poorly understood. It has been hypothesized that REE_N distribution patterns of vent fluids directly reflect the REE composition of crustal host rocks or constituent minerals, such as plagioclase, subject to alteration (Campbell et al., 1988b; Klinkhammer et al., 1994b). Alternatively, it has been proposed that REE_N distribution patterns of vent fluids reflect equilibrium partitioning between fluid and minerals, controlled primarily by fluid chemistry (e.g., pH, redox, availability of ligands), temperature, pressure and alteration mineralogy (Bau, 1991; Bach and Irber, 1998; Bach et al., 2003; Allen and Seyfried, 2005). Previous studies reporting REE compositions of submarine hydrothermal fluids have focused largely on high-temperature, black smoker fluids sampled at mid-ocean ridge hydrothermal systems, where the range of rock-types encountered by circulating fluids is limited (i.e., all are basalt-dominated) and the compositions of sampled fluids (e.g., pH, Mg, F, SO_4^{2-} concentrations, chondrite-normalized REE patterns) are generally similar. These similar characteristics make it

344 difficult to asses how REE solubility in submarine hydrothermal fluids is affected by changes in
345 fluid composition and whether aqueous REE abundances reflect that of crustal rock REE
346 compositions. In contrast, hydrothermal fluids sampled from the Manus back-arc basin have
347 interacted with crustal rocks of a wide range of composition (from basalt to dacite and rhyolite)
348 and are remarkably different in terms of their pH, fluid composition and ligand and REE
349 abundances. Accordingly, these vent fluids serve as an ideal case study by which to identify the
350 key factors that affect REE solubility at submarine hydrothermal fluids and how aqueous REE
351 abundances can be used as tracers of hydrothermal processes.
352
353 *5.1.1. Influence of Host–Rock REE Composition*
354
355 The range of REE_N distribution patterns observed in Manus Basin seafloor vent fluids do not
356 reflect variations in primary whole–rock REE abundances in basalts from the Manus Spreading
357 Center (MSC) and dacites from the Eastern Manus Basin (EMB; Figure 5). For example, light–
358 REE enriched patterns of Vienna Woods vent fluids are very different to whole–rock REE
359 distribution patterns of primary basalts erupted in the MSC (Fig. 5a). Similarly, the range of
360 REE_N distribution patterns measured in vent fluids from PACMANUS, DESMOS and SuSu
361 Knolls is different relative to the uniform whole–rock REE distribution patterns of dacites
362 erupted in the EMB (Fig. 5a). Moreover, the range of REE_N distribution patterns measured in
363 Manus Basin vent fluids do not appear to record the REE composition of specific constituent
364 minerals (see also Schnetzler and Philpotts, 1970; Hanson, 1980). In particular, the range of REE
365 fluid compositions cannot be explained as reflecting discriminate leaching of REEs from
366 plagioclase as previously suggested (Campbell et al., 1988a; Klinkhammer et al., 1994a;

Douville et al., 1999). Additional evidence suggesting that vent fluid REE abundances are not controlled by primary rock composition is provided by REE concentrations and REE_N distribution patterns that vary substantially among fluids samples within individual vent areas on spatial scales (< 100 to 500 m) over which the primary REE composition of volcanic rocks are uniform (Sinton et al., 2003; Miller et al., 2006). The fluid compositional data suggest that REEs are fractionated from primary crustal rock REE compositions during fluid–rock interaction owing to differences in aqueous REE solubility. This idea is supported by the mineral and chemical compositions of altered crustal rocks in the Manus Basin that vary significantly from chlorite–smectite (argillaceous) to illite–pyrophyllite–cristobalite–anhydrite (advanced argillic) assemblages (Lackschewitz et al., 2004; Paulick et al., 2005; Paulick and Bach, 2006; Bach et al., 2007) and indicate fluid–rock interaction involving a range of temperatures (> 220 to 360 °C), pH (< 2 to > 3.5), water/rock ratios and fluid compositions. The REE compositions of variably altered rocks show a range of chondrite–normalized compositions (Fig. 5b,c) that are consistent with variable mobilization and extensive fractionation of the REEs during crustal rock alteration (e.g., Gena et al., 2001; Beaudoin et al., 2007).

5.1.2. Influence of fluid composition – pH and Ligand Concentration

High temperature black smoker and acid–sulfate fluids in the Manus Basin exhibit a wide range of pH and fluid composition (e.g., alkali metal, Mg, Cl, F and SO_4 abundances) that reflect different styles of sub–seafloor fluid circulation, a range of conditions of fluid–rock interaction and variable crustal rock compositions (Seewald et al., 2006; Craddock, 2009; Reeves, 2010). The compositions of high–temperature black and gray smoker fluids at Vienna Woods,

390 PACMANUS and SuSu Knolls (e.g., Mg depletion and alkali metal enrichment relative to
391 ambient seawater) reflect extensive reaction (buffering) between convecting seawater–derived
392 hydrothermal fluids and fresh basalts in the MSC and dacites in the EMB (Craddock, 2009). The
393 low pH and elevated F concentrations of black smoker fluids in the EMB (PACMANUS and
394 SuSu Knolls) relative to those from the MSC (Vienna Woods) may reflect assimilation of
395 magmatic acid volatiles (H_2O–CO_2–SO_2–HCl–HF) with convecting hydrothermal fluids owing
396 to the proximity of EMB to the active subducting arc. Acid–sulfate fluids at DESMOS and SuSu
397 Knolls in the EMB are products of fundamentally different styles of hydrothermal activity and
398 are probable submarine equivalents of fumaroles associated with subaerial volcanism
399 (Giggenbach, 1992; Hedenquist et al., 1994). These fluids appear to have formed via shallow
400 mixing of magmatic acid volatiles with entrained seawater in the absence of large–scale seawater
401 convective circulation and reaction with fresh crustal rocks (Seewald et al., 2006). The low pH
402 (25 °C) < 1 to 1.5 and high sulfate concentrations (28 to 149 mmol/kg) in DESMOS and SuSu
403 Knolls acid–sulfate fluids relative to ambient seawater (Gamo et al., 1997; Seewald et al., 2006)
404 likely reflect addition of SO_2–rich magmatic vapors to seawater and disproportionation of SO_2 at
405 decreasing temperatures to yield sulfuric acid (e.g., Holland, 1965). The high concentrations of
406 Mg (≥ 24 mmol/kg) and low concentrations of fluid–mobile elements (e.g., alkali metals) in
407 acid–sulfate fluids are a critical difference relative to that of typical black smoker fluids
408 (Craddock, 2009). These data suggest that acid-sulfate fluid compositions are not governed
409 primarily by reaction with fresh crustal rocks, but reflect interaction with previously and variably
410 altered crustal rocks. This idea is supported by the occurrence of highly altered rocks containing
411 cristobalite, alunite, pyrophyllite and native sulfur in proximity to acid–sulfate fluids at the
412 seafloor at DESMOS and SuSu Knolls (Gamo et al., 1997; Bach et al., 2007) that are analogous

413 to the low pH, advanced–argillic alteration observed in subaerial epithermal environments
414 (Hemley and Jones, 1964; Hemley et al., 1969).
415
416 We propose that the range of REE abundances observed in Manus Basin hydrothermal fluids are
417 controlled primarily by fluid composition (e.g., pH, availability of ligands) and alteration
418 mineralogy, which regulate aqueous REE solubility during sub–seafloor fluid–rock interaction.
419 Overall, REE concentrations in Manus Basin vent fluids increase with acidity (Fig. 6). REE
420 concentrations in acid–sulfate fluids from DESMOS and SuSu Knolls are high relative to black
421 and gray smoker fluids sampled in the Manus Basin, despite the lower temperatures of acid–
422 sulfate fluids. Similarly, REE concentrations are high in lower pH smoker fluids from
423 PACMANUS and SuSu Knolls (pH (25 °C) 2.3 to 3.5) relative to higher pH smoker fluids
424 sampled from Vienna Woods (pH (25 °C) $\geq$ 4.2). Similar correlations in hydrothermal fluids
425 sampled from a range of geologic environments, including basalt–dominated mid–ocean ridge
426 (MOR) and continental geothermal systems (Michard and Albarede, 1986; Michard, 1989; Lewis
427 et al., 1997; Douville et al., 1999; Wood, 2001) support this relationship. It is unlikely that REE
428 abundances in seafloor hydrothermal fluids are limited by their abundance in the host rock
429 because the concentrations of REEs in both fresh and altered oceanic crustal rocks (e.g., Michard
430 et al., 1983; Beaudoin et al., 2007) are several orders of magnitude higher than those measured in
431 submarine hydrothermal fluids (see Fig. 5). Indeed, acid–sulfate fluids have the highest REE
432 concentrations, despite these fluids having bulk aqueous compositions consistent with reaction
433 with altered crustal rocks, which typically contain REE abundances lower than those in primary
434 igneous lavas (e.g., Beaudoin et al., 2007). The results suggest total REE abundances in
435 submarine hydrothermal fluids are solubility controlled during high–temperature fluid–rock

436 interaction, are strongly influenced by pH, and are largely independent of crustal–rock REE
437 abundances.
438
439 Sampled vent fluids are also characterized by a range of chondrite-normalized (REE_N) patterns
440 that vary systematically with pH and the availability of aqueous ligands. These trends are readily
441 apparent upon examination of La_N/Yb_N and Eu_N/Eu^*_N ratios as a function of relative ligand
442 abundances (Fig. 7). The La_N/Yb_N ratio is a measure of the relative light–REE (La) versus
443 heavy–REE (Yb) abundance and reflects chemical fractionation among the light– and heavy–
444 REEs. The Eu_N/Eu^*_N ratio (Eu anomaly) is a measure of the fractionation of Eu relative to
445 neighboring REEs (Sm and Gd), which can be related to the varying oxidation state exhibited by
446 Eu (II and III) compared to trivalent REEs in high–temperature hydrothermal fluids (Sverjensky,
447 1984). High–temperature smoker fluids from all Manus Basin vent areas exhibit a wide range of
448 $\Sigma F/\Sigma Cl$ ratios and a limited range of low $\Sigma SO_4/\Sigma Cl$ ratios, the latter being the result of sulfate
449 removal by anhydrite precipitation and reduction to H_2S during fluid–rock interaction. Manus
450 Basin smoker fluids with low F and SO_4^{2-} concentrations, and low $\Sigma F/\Sigma Cl$ (< 0.03 μM/mM) and
451 $\Sigma SO_4/\Sigma Cl$ ratios (~ 1 μM/mM) have a characteristic light-REE enrichment and large positive Eu-
452 anomaly (highest La_N/Yb_N and Eu_N/Eu^*_N ratios; Fig. 7). In contrast, smoker fluids that have a
453 range of high F concentrations and high $\Sigma F/\Sigma Cl$ ratios have only minor light-REE enrichments
454 and lower La_N/Yb_N and Eu_N/Eu^*_N ratios. The most fluoride-rich sampled fluids with the highest
455 $\Sigma F/\Sigma Cl$ ratios approaching ~ 0.60 – 0.80 μM/mM (Satanic Mills SM2, Fenway F1, Suzette SZ5;
456 Table 1, Fig. 7) exhibit a distinct light-REE depletion and heavy–REE enrichment (La_N/Yb_N <<
457 1) and a small or absent Eu anomaly (Eu_N/Eu^*_N ~ 1 to 2).
458

We interpret the range of light- versus heavy-REE enrichments observed in these fluids as reflecting differences in relative solubilities of the light- versus heavy-REEs as a direct result of significant differences in pH, ligand concentration and, therefore, the relative abundances of REE-chloride and REE-fluoride complexes. The pronounced light-REE enrichment and positive Eu-anomaly in smoker fluids with chloride–rich, but fluoride– and sulfate–poor compositions implies that REE-chloride complexation acts to enhance the solubility of the light-REEs and Eu relative to that of the mid- and heavy-REEs during fluid–rock interaction and secondary mineral formation. In contrast, the marked heavy-REE enrichment in fluoride-rich smoker fluids suggests that formation of REE-fluoride complexes enhances the solubility of the heavy-REEs relative to light-REEs during fluid-rock interaction in the presence of elevated concentrations of fluoride.

These interpretations are supported by the results of species distribution thermodynamic calculations that were carried out to assess the aqueous speciation/complexation of REEs in representative sampled Manus hydrothermal fluids at in situ temperature and pressure across a broad range of fluid compositions (compositions of the 7 fluids used for illustration in speciation calculations are given Table 3; results of calculations are presented in Fig. 8). Details of the thermodynamic calculations used in this study are documented in full in the Supporting Online Material (SOM). Briefly, calculations were carried out using the SpecE8 program, included as a module of the Geochemist's Workbench (v6.0) software package (Bethke, 1996). The SpecE8 program computes species distributions, mineral saturation states and gas fugacity in aqueous solutions at specified temperature and pressure. The thermodynamic database used in SpecE8 calculations was generated using SUPCRT92 (Johnson et al., 1992) for a pressure of 50 MPa (500 bars) and temperatures between 0 and 400 °C, using updates for aqueous formation

constants as listed in the SOM. The pH value of each fluid measured at 25 °C was used together with aqueous compositional data to calculate pH at in situ temperature. The redox potential for each fluid was calculated based on measured H_2(aq) concentrations and the assumption of H_2(aq)-H_2O equilibrium. Equilibrium between H_2S and SO_4^{2-} was suppressed because both species were measured in our hydrothermal fluids and are in a state of non-equilibrium. REE speciation in chloride-rich, but fluoride- (< 20 to 170 μmol/kg) and sulfate-poor (< 2 mmol/kg) smoker-type vent fluids is governed primarily by REE-chloride and REE-oxyhydroxide complexes of trivalent REEs and chloride complexes of divalent Eu (e.g., Vienna Woods VW1, Roman Ruins RMR4, Satanic Mills SM1; Fig. 8). REE–fluoride complexes are present in lesser amounts and REE–sulfate complexes are present at relatively low abundance. The predominance of divalent Eu versus trivalent Eu reflects the stability of Eu^{2+} under reducing conditions and elevated temperatures characteristic of sampled vent fluids (e.g., Sverjensky, 1984). The differences in the relative abundance of REE–chloride and REE–oxyhydroxide complexes result primarily from differences in fluid temperature and pH with REE–chloride complexes increasing in abundance at higher temperature and lower pH. The calculated REE speciation does not change significantly across different geologic settings and crustal compositions (e.g., basalt–dominated Vienna Woods versus dacite–dominated PACMANUS) because the fluid compositions are similar.

REE species distribution in high-temperature vent fluids with a range of elevated fluoride concentrations (up to ~ 500 μmol/kg) is increasingly governed by the presence of REE-fluoride complexes, which occur primarily at the expense of REE-chloride complexes (e.g., Satanic Mills SM2, Suzette SZ5, Fig. 8). The light–REEs occur predominantly as chloride complexes, but the

heavy–REEs are present predominantly as fluoride complexes. The relative abundance of REE–hydroxide and REE–sulfate complexes are low; similar to that predicted for other high-temperature smoker fluids. Europium is again predicted to occur exclusively as a divalent chloride complex. Theoretical and experimental estimates of the relative stabilities of REE-chloride and REE-fluoride complexes across the lanthanide group (e.g., Wood, 1990; Haas et al., 1995; Gammons et al., 2002; Migdisov and Williams-Jones, 2007; Migdisov et al., 2009) are not without uncertainties and discrepancies (see documentation of thermodynamic data in SOM). However, these studies suggest that chloride complexes of the light-REEs and Eu^{2+} are more stable than those of the heavy-REEs at elevated temperature and pressure, whereas fluoride complexes possibly show the opposite behavior, consistent with our interpretation of natural samples. Fractionation of the REEs during fluid-rock interaction and secondary mineral formation owing to differences in complexation and solubility of the REEs is also consistent with the results of experimental studies that have demonstrated enhanced mobility of the light–REEs and divalent Eu^{2+} during fluid–rock interaction with chloride–rich hydrothermal fluids at elevated temperature and pressure (e.g., Allen and Seyfried, 2005). No experimental studies have yet investigated the relative solubility and mobility of the REEs during fluid-rock interaction in the presence of fluoride-rich hydrothermal fluids at elevated temperature and pressure.

Marked differences in fluid composition likely also govern the REE distributions observed in acid-sulfate fluids, which are distinct to those of smoker fluids. All acid–sulfate fluids exhibit almost flat REE_N distribution patterns with no Eu-anomalies ($La_N/Yb_N \sim 1$ to 2.5, $Eu_N/Eu^*_N \sim 1$), similar to REE_N patterns identified in other acid–sulfate fluids sampled in the Manus Basin (e.g., Douville et al., 1999). We interpret the high REE concentrations and flat REE_N patterns of acid–

sulfate fluids as reflecting primarily the influence of low pH, which enhances the aqueous solubility of *all* REEs. The very low pH is likely the critical parameter controlling the observed abundances of REEs in acid-sulfate fluids because observations of natural systems suggest that the solubility of REEs during fluid-rock reaction increases significantly with acidity (Fig. 6) (e.g., Michard, 1989; Lewis et al., 1998; Fulignati et al., 1999). In effect, acid-sulfate-type alteration occurring at very low pH, as is observed at DESMOS and SuSu Knolls, effectively leaches and mobilizes REEs from host rocks without fractionation among the lanthanides. Indeed, REE_N distribution patterns of acid-sulfate fluids are similar to that of both primary and altered felsic crustal rocks in the Eastern Manus Basin (e.g., Gena et al., 2001) with which acid-sulfate fluids have likely reacted (Fig. 5c).

Results of thermodynamic species distribution calculations suggest that formation of aqueous REE complexes in acid-sulfate fluids appears to exert a relatively minor control over the relative solubility of the REEs. REE species distribution calculations suggest that at lower temperatures relevant to most acid-sulfate fluids (< 120 °C) the REEs are present in solution predominantly as free trivalent ions (e.g., DESMOS D1, Fig. 8). Similar results were obtained in REE species distribution calculations reported for acid-sulfate fluid by Douville et al. (1999) and Bach et al. (2003). Europium can occur as trivalent Eu reflecting the lower temperature and more oxidizing composition of these fluids relative to typical high-temperature smoker fluids. A low pH is critical for maintaining high concentrations of REEs in solution as uncomplexed ions. The formation of REE-sulfate complexes as predicted by species distribution calculations (owing to high sulfate concentrations in acid-sulfate fluids up to 150 mmol/kg) may further enhance REE solubility. At higher temperatures (> 200 °C), thermodynamic calculations predict that REE-

chloride complexes increasingly contribute to REE speciation in acid-sulfate fluids (e.g., North Su NS2; Fig. 8). Differences in the relative abundance of REE-sulfate versus REE-chloride complexes do not obviously affect overall REE abundances, suggesting that pH is the more important control. Measured REE abundances and REE_N patterns are not obviously affected by the wide range of fluoride concentrations in acid-sulfate fluids (Fig. 7), suggesting that REE-fluoride complexes do not contribute to aqueous REE speciation in these fluids. The lack of REE-fluoride complexation in acid-sulfate fluids (Figs. 8 and 9) likely reflects quantitative sequestration of fluoride as HF° at very low pH owing to the weak acid behavior of hydrofluoric acid at elevated temperature (pKa ~ 3.1 at 25 °C and 4.6 at 200 °C). It has also been suggested that competitive formation of Al–fluoride complexes may inhibit REE-fluoride complex formation in acid-sulfate fluids (Gimeno Serrano et al., 2000). Indeed, acid–sulfate fluids sampled in the Manus Basin have very high concentrations of dissolved Al (Table 3) and Al-fluoride complexes and HF° constitute the entirety of aqueous fluoride species in acid-sulfate fluids (Fig. 9). The presence or absence of Al-fluoride complexes, however, does not affect the predicted abundance of REE-fluoride complexes in acid-sulfate fluids because formation of Al–fluoride complexes in acid–sulfate fluids occurs predominantly at the expense of HF°, not REE–fluoride complexes (Fig. 9).

In summary, the data presented suggest that REE solubility during fluid–rock interaction at elevated temperature and pressure is critically dependent upon fluid composition – in particular pH and the concentration of aqueous REE ligands. Different REE abundances and REE_N distribution patterns among smoker– and acid–sulfate–type fluids in the Manus Basin likely reflect differences in REE solubility owing to variations in the relative abundance and stability of

574 REE–chloride, fluoride and sulfate complexes as a function of different temperature, pH and
575 ligand concentration (e.g., ΣF/ΣCl and $\Sigma SO_4/\Sigma Cl$ ratios). The observed correlations suggest that
576 light–REE and Eu enrichments (large positive La_N/Yb_N and Eu_N/Eu^*_N ratios) are favored in
577 hydrothermal fluids with low fluoride and sulfate concentrations (low ΣF/ΣCl and $\Sigma SO_4/\Sigma Cl$
578 ratios) in which REE–chloride complexes are the likely dominant REE species. In contrast,
579 heavy–REE (and to a lesser degree mid–REE) enrichments are favored in hydrothermal fluids
580 with high fluoride concentrations (high ΣF/ΣCl ratios) in which REE–fluoride complexes are
581 likely important REE species. In acid–sulfate fluids, enrichment of all REEs appears to be
582 critically dependent upon the very low pH and possibly, to a lesser extent, the presence of REE–
583 sulfate and/or chloride complexes. Importantly, the apparent sensitivity of aqueous REE
584 distributions to pH and Cl, F and SO_4^{2-} concentrations implies that the REEs can be used as
585 tracers for input of fluoride– and sulfur–rich magmatic acid volatiles (H_2O–CO_2–SO_2–HCl–HF)
586 in seafloor hydrothermal fluids. Further, because minerals in hydrothermal vent deposits (e.g.,
587 anhydrite) often record REE distributions which preserve that of the original hydrothermal fluid,
588 the REEs may also provide critical information about hydrothermal processes associated with the
589 formation of seafloor vent deposits, such as fluid pH, composition and the extent and type of
590 magmatic acid volatile input, all of which impact metal behavior and metal-sulfide
591 mineralization.
592
593 *5.1.3. Consequences of Seawater Entrainment and Fluid Mixing*
594
595 Studies of MOR hydrothermal systems have demonstrated that entrainment and sub–seafloor
596 mixing of seawater with rising high–temperature hydrothermal fluids can affect seafloor vent

597 fluid compositions owing to mineral precipitation and/or dissolution (Edmond et al., 1995; Tivey
598 et al., 1995). Anhydrite ($CaSO_4$) precipitation is a common product of sub–seafloor mixing
599 between high–temperature fluids and locally entrained seawater (Tivey et al., 1995; Mills et al.,
600 1998; Tivey et al., 1998; Mills and Tivey, 1999; Humphris and Bach, 2005) and can incorporate
601 significant amounts of REEs (Mills and Elderfield, 1995; Humphris, 1998). Substantial amounts
602 of anhydrite have been recovered from beneath several PACMANUS vent deposits (Binns et al.,
603 2007; Tivey et al., 2007). The down–hole distribution of anhydrite veins in Ocean Drilling
604 Program Leg 193 drill core from PACMANUS demonstrates widespread precipitation of
605 anhydrite extending to depths > 300 mbsf (Bach et al., 2003; Roberts et al., 2003). Sulfate–sulfur
606 isotopic compositions of anhydrite at PACMANUS cluster around that of seawater sulfate
607 consistent with deposition of anhydrite in response to sub–seafloor mixing between entrained
608 seawater and high–temperature hydrothermal fluid (Roberts et al., 2003; Craddock et al., 2010).
609
610 The range of chemical compositions of seafloor vent fluids sampled at PACMANUS is
611 consistent with ongoing anhydrite precipitation at some vent areas (Seewald et al., 2006; Reeves,
612 2010). The highest temperature (≥ 340 °C) fluids sampled at PACMANUS have near zero Mg
613 and sulfate concentrations, whereas lower temperature (< 280 °C) smoker fluids exhibit a range
614 of higher Mg and sulfate concentrations consistent with mixing between end–member high–
615 temperature hydrothermal fluids and locally entrained Mg– and sulfate–rich seawater (Reeves,
616 2010)(Table 1; Fig. 10). Measured sulfate concentrations in most lower temperature fluids are,
617 however, significantly less than that predicted by conservative mixing between end–member
618 hydrothermal fluid (zero Mg and SO_4) and ambient seawater causing measured sulfate
619 concentrations to extrapolate to negative values at zero Mg. Although the value has no true

620 physical meaning, the magnitude of the negative end–member concentration represents a proxy
621 for the extent of non–conservative sulfate removal during fluid mixing. Lower temperature fluids
622 also exhibit Ca concentrations less than that predicted by conservative mixing between end–
623 member hydrothermal fluid and ambient seawater (Fig. 10b). The extent of non–conservative Ca
624 removal is correlated with that of sulfate (Fig. 10c) and is explained by anhydrite precipitation
625 during near–seafloor mixing of high temperature hydrothermal fluids and locally entrained
626 seawater. The REEs exhibit non–conservative behavior similar to Ca during fluid mixing
627 suggesting that anhydrite precipitation has caused measurable removal of aqueous REEs (Fig.
628 10d). On the basis of the observed correlations and the magnitude of the negative sulfate end–
629 member concentrations, ongoing deposition of anhydrite appears most prevalent at the Snowcap
630 and Roman Ruins (PACMANUS) vent areas.
631
632 Measured Mg concentrations in low temperature (~ 78 °C) fluids exiting diffusely from the
633 seafloor at Fenway (fluid F5) are near seawater concentration and are consistent with large–scale
634 entrainment of seawater by ascending high–temperature hydrothermal fluids within the Fenway
635 mound (Table 1). Sulfate and Ca concentrations in these diffuse fluids are higher than that
636 predicted by conservative mixing between parent high–temperature hydrothermal fluids and
637 seawater (Fig 10a, b), suggesting that local dissolution of previously deposited anhydrite is on–
638 going in some fluids at Fenway in response to low fluid temperatures that enhance anhydrite
639 solubility (Bischoff and Seyfried, 1978). Dissolution of anhydrite yields end–member sulfate and
640 Ca concentrations in diffuse fluids that are higher than in the highest–temperature black smoker
641 fluids at zero Mg (Fig. 10c). End–member REE concentrations in diffuse fluids at Fenway are
642 also higher than in parent high–temperature vent fluids (Fig. 10d) and are interpreted as

643 reflecting addition of REEs to solution as a result of anhydrite dissolution. It should be
644 recognized that high end–member concentrations of sulfate, Ca and REEs in diffuse fluids are an
645 artifact of extrapolation to zero Mg and should not be interpreted as indicating the actual
646 existence of a high–temperature fluid with the specified zero Mg composition. Anhydrite
647 dissolution represents a potential significant source of REEs because total REE concentrations in
648 massive anhydrites recovered at the seafloor at Fenway reach values as high as 50 ppm and are
649 enriched by several orders of magnitude relative to total REE concentrations in high–temperature
650 hydrothermal fluids (Craddock et al., 2010). The REE_N patterns of high– and low–temperature
651 hydrothermal fluids and of massive anhydrites at Fenway are similar (Craddock et al., 2010)
652 indicating that dissolution of anhydrite does not, however, affect relative REE_N distributions
653 among the sampled Fenway vent fluids.
654

655 ## 6. SUMMARY AND CONCLUSIONS

656

657 Rare earth element data are reported for a wide range of seafloor vent fluids sampled from four
658 hydrothermal systems in the Manus back–arc basin (Vienna Woods, PACMANUS, DESMOS
659 and SuSu Knolls). Chondrite–normalized REE_N distribution patterns of Manus vent fluids show
660 a wide range of compositions, which contrast with the uniform REE_N distribution patterns of
661 mid–ocean ridge (MOR) hydrothermal fluids. These differences are correlated with differences
662 in fluid composition, in particular pH and ligand (chloride, fluoride and sulfate) abundances.
663 Vent fluid REE_N distribution patterns are not obviously correlated to differences in crustal rock
664 REE compositions. The results imply that REE compositions of hydrothermal fluids are
665 controlled predominantly by conditions of fluid–rock interaction (i.e., pH, temperature,

availability of complexing ligands), which affect the relative solubility and mobilization of the REEs. Our data are supported by experimental studies that have documented fractionation of the REEs during high–temperature fluid–rock reaction (e.g., Bach and Irber, 1998; Allen and Seyfried, 2005).

In the Manus Basin, the range of REE_N patterns observed in seafloor vent fluids is interpreted as reflecting heterogeneous solubility/mobility of the REEs during fluid–rock interaction owing to the formation of REE–chloride, REE–fluoride and REE–sulfate complexes with a range of aqueous stabilities. The range of fluoride and sulfate concentrations measured in Manus hydrothermal fluids is attributed to differing amounts and styles of magmatic acid volatile (i.e., H_2O–CO_2–HCl–HF–SO_2) degassing (Gamo et al., 1997; Douville et al., 1999; Seewald et al., 2006; Reeves, 2010). A significant implication of our results are that REE distributions in seafloor hydrothermal fluids can be used as indicators of styles of magmatic degassing at depth. It has been proposed that the uniform REE_N pattern of MOR hydrothermal fluids (i.e., light–REE enrichment and positive Eu anomaly) primarily reflects exchange of REE during plagioclase recrystallization (Campbell et al., 1988b; Klinkhammer et al., 1994b; Douville et al., 1999). The results of this study, however, suggest that a light–REE enrichment and positive Eu anomaly reflect enhanced mobility of the light–REEs and Eu owing to the predominance of REE–chloride complexes in chloride–rich and fluoride– and sulfate–poor MOR hydrothermal fluids. Local processes, including sub–surface fluid mixing and mineral deposition and remobilization, may also affect REE concentrations of seafloor hydrothermal fluids. However, REE_N distributions of seafloor vent fluids are primarily affected by key aspects of fluid composition (e.g., pH, ligand concentration) that affect REE speciation and mobility during fluid–rock interaction at depth.

This detailed study of REE compositions of seafloor vent fluids indicates that REEs can provide critical information about fundamental sub–seafloor geochemical processes associated with hydrothermal activity, including conditions of fluid–rock interaction and the extent and styles of magmatic acid volatile degassing. A better understanding of aqueous REE behavior offers important constraints for interpreting REE signatures preserved in the mineral record. Future studies of REE–bearing mineral deposits can be used to gain insight about geochemical processes pertaining to hydrothermal vent deposit formation and are essential for inactive and relict systems where access to hydrothermal fluids is precluded.

ACKNOWLEDGMENTS

The authors acknowledge the Captain and crew of the *R/V Melville* and the *ROV Jason II* technical group for a very successful cruise and sample collection. P. Saccocia and E. Walsh provided great help during shipboard fluid sample processing. D. Schneider and S. Birdwhistell (WHOI) are acknowledged for assistance during rare earth element analysis by ICP–MS. Reviews by A.A. Migdisov and an anonymous reviewer provided critical, constructive and thought-provoking comments that greatly aided in the discussion and presentation of our research. The authors thank the Associate Editor, J.-I. Ishibashi, for his editorial assistance and supportive and insightful comments. This study received financial support from the Ocean Drilling Program Schlanger Fellowship (to P.R. Craddock), the WHOI Deep Ocean Exploration Institute Graduate Fellowship (to E. Reeves) and NSF grant OCE–0327448.

REFERENCES

Allen D. E. and Seyfried W. E., Jr. (2005) REE controls in ultramafic hosted MOR hydrothermal systems: An experimental study at elevated temperature and pressure. *Geochimica et Cosmochimica Acta* **69**(3), 675-683.

Bach W. and Irber W. (1998) Rare earth element mobility in the oceanic lower sheeted dyke complex: evidence from geochemical data and leaching experiments. *Chemical Geology* **151**(1), 309-326.

Bach W., Roberts S., Vanko D. A., Binns R. A., Yeats C. J., Craddock P. R., and Humphris S. E. (2003) Controls of fluid chemistry and complexation on rare-earth element contents of anhydrite from the Pacmanus subseafloor hydrothermal system, Manus Basin, Papua New Guinea. *Mineralium Deposita* **38**(8), 916-935.

Bach W., Tivey M. A., Seewald J. S., Tivey M. K., Craddock P. R., Niedermeier D., and Yoerger D. (2007) Variable basement compostion and magma degassing affecting hydrothermal systems in the Eastern Manus Basin. *EOS Trans. AGU. Fall Meet. Suppl.,* **88**(52), Abstract #V21D-0749.

Bau M. (1991) Rare-earth element mobility during hydrothermal and metamorphic fluid-rock interaction and the significance of the oxidation state of europium. *Chemical Geology* **93**(3-4), 219-230.

Bau M. and Dulski P. (1999) Comparing yttrium and rare earths in hydrothermal fluids from the Mid-Atlantic Ridge: implications for Y and REE behaviour during near-vent mixing and for the Y/Ho ratio of Proterozoic seawater. *Chemical Geology* **155**(1), 77-90.

Beaudoin Y., Scott S. D., Gorton M. P., Zajacz Z., and Halter W. (2007) Effects of hydrothermal alteration on Pb in the active PACMANUS hydrothermal field, ODP Leg 193, Manus Basin, Papua New Guinea: A LA-ICP-MS study. *Geochimica et Cosmochimica Acta* **71**(17), 4256-4278.

737 Bethke C. M. (1996) *Geochemical Reaction Modeling*. Oxford University Press.
738 Binns R. A., Barriga F. J. A. S., and Miller D. J. (2007) Leg 193 synthesis: Anatomy of an active
739 felsic-hosted hydrothermal system, eastern Manus Basin, Papua New Guinea. In
740 *Proceedings of the Ocean Drilling Program, Scientific Results*, Vol. 193 (ed. F. J. A. S.
741 Barriga, R. A. Binns, D. J. Miller, and P. M. Herzig), pp. 1-71.
742 doi:10.2973/odp.proc.sr.193.201.2007. Ocean Drilling Program.
743 Binns R. A. and Scott S. D. (1993) Actively forming polymetallic sulfide deposits associated
744 with felsic volcanic rocks in the eastern Manus back-arc basin, Papua New Guinea.
745 *Economic Geology* **88**, 2226-2236.
746 Binns R. A., Scott S. D., Gemmell J. B., Crook K. A. W., and Shipboard Scientific Party. (1997)
747 The SuSu Knolls hydrothermal field, eastern Manus Basin, Papua New Guinea. *EOS*
748 *Trans. AGU. Fall Meet. Suppl.,* **78**(52), Abstract #V22E-02.
749 Bischoff J. L. and Seyfried W. E., Jr. (1978) Hydrothermal chemistry of seawater from 25° to
750 350°C. *American Journal of Science* **278**, 838-860.
751 Both R., Crook K., Taylor B., Brogan S., Chappell B., Frankel E., Liu L., Sinton J., and Tiffin D.
752 (1986) Hydrothermal chimneys and associated fauna in the Manus back-arc basin, Papua
753 New Guinea. *EOS Transactions, American Geophysical Union* **67**, 489.
754 Campbell A. C., Bowers T. S., Measures C. I., Falkner K. K., Khadem M., and Edmond J. M.
755 (1988a) A time series of vent fluid compositions from 21 °N, East Pacific Rise (1979,
756 1981, 1985), and the Guaymas Basin, Gulf of California (1982, 1985). *Journal of*
757 *Geophysical Research* **93**(B5), 4537-4549.
758 Campbell A. C., Palmer M. R., Klinkhammer G. P., Bowers T. S., Edmond J. M., Lawrence J.
759 R., Casey J. F., Thompson G., Humphris S. E., and Rona P. (1988b) Chemistry of hot
760 springs on the Mid-Atlantic Ridge. *Nature* **335**(6190), 514-519.
761 Craddock P. R. (2009) Geochemical Tracers of Processes Affecting the Formation of Seafloor
762 Hydrothermal Fluids and Deposits in the Manus Back-arc Basin. Ph. D. Thesis,
763 Massachusetts Institute of Technology-Woods Hole Oceanographic Institution, Woods

764 Hole, MA, 370 pp.
765 Craddock P. R., Bach W., and Rosner M. (2010) Insights to magmatic–hydrothermal processes
766 in the Manus back-arc basin as recorded by anhydrite. *Geochimica et Cosmochimica*
767 *Acta*.
768 Davies H. L., Honza E., Tiffin D. L., Lock J., Okuda Y., Keene J. B., Murakami F., and
769 Kisimoto K. (1987) Regional setting and structure of the western Solomon Sea. *Geo-*
770 *Marine Letters* **7**, 153-160.
771 Douville E., Bienvenu P., Charlou J. L., Donval J. P., Fouquet Y., Appriou P., and Gamo T.
772 (1999) Yttrium and rare earth elements in fluids from various deep-sea hydrothermal
773 systems. *Geochimica et Cosmochimica Acta* **63**(5), 627-643.
774 Edmond J. M., Campbell A. C., Palmer M. R., German C. R., Klinkhammer G. P., Edmonds H.
775 N., Elderfield H., Thompson G., and Rona P. (1995) Time series studies of vent fluids
776 from the TAG and MARK sites (1986, 1990) Mid-Atlantic Ridge and a mechanism for
777 Cu/Zn zonation in massive sulphide orebodies. In *Hydrothermal Vents and Processes*,
778 Vol. 87 (ed. L. M. Parson, C. L. Walker, and D. R. Dixon), pp. 77-86. Geological Society
779 Special Publication.
780 Fulignati P., Gioncada A., and Sbrana A. (1999) Rare-earth element (REE) behaviour in the
781 alteration facies of the active magmatic-hydrothermal system of Vulcano (Aeolian
782 Islands, Italy). *Journal of Volcanology and Geothermal Research* **88**(4), 325-342.
783 Gammons C. H., Wood S. A., and Youning L. (2002) Complexation of the rare earth elements
784 with aqueous chloride at 200 °C and 300 °C and saturated water vapor pressure. In
785 *Water-Rock Interaction, Ore Deposits and Environmental Geochemistry: A Tribute to*
786 *David A. Crerar. The Geochemical Society Special Publication*, Vol. 7 (ed. R. Hellmann
787 and S. A. Wood), pp. 191–207.
788 Gamo T., Okamura K., Charlou J. L., Urabe T., Auzende J. M., Ishibashi J.-I., Shitashima K.,
789 Chiba H., Binns R. A., and Gena K. (1997) Acidic and sulfate-rich hydrothermal fluids
790 from the Manus back-arc basin, Papua New Guinea. *Geology* **25**(2), 139-142.

791 Gena K., Mizuta T., Ishiyama D., and Urabe T. (2001) Acid-sulphate type alteration and
792 mineralization in the Desmos Caldera, Manus back-arc basin, Papua New Guinea.
793 *Resource Geology* **51**(1), 31-44.
794 Giggenbach W. F. (1992) Isotopic shifts in waters from geothermal and volcanic systems along
795 convergent plate boundaries and their origin. *Earth and Planetary Science Letters* **113**,
796 495-510.
797 Gimeno Serrano M. J., Auque Sanz L. F., and Nordstrom D. K. (2000) REE speciation in low-
798 temperature acidic waters and the competitive effects of aluminum. *Chemical Geology*
799 **165**(3-4), 167-180.
800 Haas J. R., Shock E. L., and Sassani D. C. (1995) Rare earth elements in hydrothermal systems:
801 Estimates of standard partial molal thermodynamic properties of aqueous complexes of
802 the rare earth elements at high pressures and temperatures. *Geochimica et Cosmochimica*
803 *Acta* **59**(21), 4329-4350.
804 Hanson G. N. (1980) Rare Earth Elements in petrogenetic studies of igneous systems. *Annual*
805 *Review of Earth and Planetary Sciences* **8**(1), 371-406.
806 Hedenquist J. W., Aoki M., and Shinohara H. (1994) Flux of volatiles and ore-forming metals
807 from the magmatic-hydrothermal system of Satsuma Iwojima Volcano. *Geology* **22**(7),
808 585-588.
809 Hemley J. J., Hostetler P. B., Gude A. J., and Mountjoy W. T. (1969) Some stability relations of
810 alunite. *Economic Geology* **64**, 599-612.
811 Hemley J. J. and Jones W. R. (1964) Chemical aspects of hydrothermal alteration with emphasis
812 on hydrogen metasomatism. *Economic Geology* **59**(538-569).
813 Holland H. D. (1965) Some applications of thermochemical data to problems of ore deposits; [II]
814 Mineral assemblages and the composition of ore forming fluids. *Economic Geology*
815 **60**(6), 1101-1166.
816 Hrischeva E., Scott S. D., and Weston R. (2007) Metalliferous sediments associated with
817 presently forming volcanogenic massive sulfides: The SuSu Knolls hydrothermal field,

Eastern Manus Basin, Papua New Guinea. *Economic Geology* **102**, 55-74.

Humphris S. E. (1998) Rare earth element composition of anhydrite: Implications for deposition and mobility within the TAG hydrothermal mound. In *Proceedings of the Ocean Drilling Program, Scientific Results*, Vol. 158 (ed. P. M. Herzig, S. E. Humphris, D. J. Miller, and R. A. Zierenberg), pp. 143-159. Ocean Drilling Program.

Humphris S. E. and Bach W. (2005) On the Sr isotope and REE compositions of anhydrites from the TAG seafloor hydrothermal system. *Geochimica et Cosmochimica Acta* **69**, 1511-1525.

Johnson J. W., Oelkers E. H., and Helgeson H. C. (1992) SUPCRT92: a software package for calculating the standard molal thermodynamic properties of minerals, gases, aqueous species and reactions from 1 to 5000 bar, and 0 to 1000 °C. *Computers and Geosciences* **18**(7), 899-947.

Klinkhammer G., German C. R., Elderfield H., Greaves M. J., and Mitra A. (1994a) Rare earth elements in hydrothermal fluids and plume particulates by inductively coupled plasma mass spectrometry. *Marine Chemistry* **45**(3), 179-186.

Klinkhammer G. P., Elderfield H., Edmond J. M., and Mitra A. (1994b) Geochemical implications of rare earth element patterns in hydrothermal fluids from mid-ocean ridges. *Geochimica et Cosmochimica Acta* **58**(23), 5105-5113.

Lackschewitz K. S., Devey C. W., Stoffers P., Botz R., Eisenhauer A., Kummetz M., Schmidt M., and Singer A. (2004) Mineralogical, geochemical and isotopic characteristics of hydrothermal alteration processes in the active, submarine, felsic-hosted PACMANUS field, Manus Basin, Papua New Guinea. *Geochimica et Cosmochimica Acta* **68**(21), 4405-4427.

Lewis A. J., Komninou A., Yardley B. W. D., and Palmer M. R. (1998) Rare Earth Element Speciation in Geothermal Fluids from Yellowstone National Park, Wyoming, USA. *Geochimica et Cosmochimica Acta* **62**(4), 657-663.

Lewis A. J., Palmer M. R., Sturchio N. C., and Kemp A. J. (1997) The rare earth element

geochemistry of acid-sulphate and acid-sulphate-chloride geothermal systems from Yellowstone National Park, Wyoming, USA. *Geochimica et Cosmochimica Acta* **61**(4), 695-706.

Martinez F. and Taylor B. (1996) Backarc spreading, rifting, and microplate rotation, between transform faults in the Manus Basin. *Marine Geophysical Researches* **18**, 203-224.

Michard A. (1989) Rare earth element systematics in hydrothermal fluids. *Geochimica et Cosmochimica Acta* **53**, 745-750.

Michard A. and Albarede F. (1986) The REE content of some hydrothermal fluids. *Chemical Geology* **55**(1-2), 51-60.

Michard G., Albarède F., Michard A., Minster J. F., and Charlou J. L. (1983) Rare-earth elements and uranium in high-temperature solutions from East Pacific Rise hydrothermal vent field (13 °N). *Nature* **303**(795-797).

Migdisov A. A. and Williams-Jones A. E. (2007) An experimental study of the solubility and speciation of NdF_3 in F-bearing aqueous solutions. *Geochimica et Cosmochimica Acta* **71**, 3056-3069.

Migdisov A. A., Williams-Jones A. E., and Wagner T. (2009) An experimental study of the solubility and speciation of the Rare Earth Elements (III) in fluoride- and chloride-bearing aqueous solutions at temperatures up to 300 °C. *Geochimica et Cosmochimica Acta* **73**, 7087-7109.

Miller D. J., Vanko D. A., and Paulick H. (2006) Data Report: Petrology and geochemistry of fresh, recent dacite lavas at Pual Ridge, Papua New Guinea, from an active, felsic-hosted seafloor hydrothermal system. In *Proceedings of the Ocean Drilling Program, Scientific Results*, Vol. 193 (ed. F. J. A. S. Barriga, R. A. Binns, D. J. Miller, and P. M. Herzig), pp. 1-31. doi:10.2973/odp.proc.sr.193.208.2006. Ocean Drilling Program.

Mills R. A. and Elderfield H. (1995) Rare earth element geochemistry of hydrothermal deposits from the active TAG Mound, 26 °N Mid-Atlantic Ridge. *Geochimica et Cosmochimica Acta* **59**, 3511-3524.

872 Mills R. A., Teagle D. A. H., and Tivey M. K. (1998) Fluid mixing and anhydrite precipitation
873 within the TAG mound. In *Proceedings of the Ocean Drilling Program, Scientific*
874 *Results*, Vol. 158 (ed. P. M. Herzig, S. E. Humphris, D. J. Miller, and R. A. Zierenberg),
875 pp. 119-127. Ocean Drilling Program.
876 Mills R. A. and Tivey M. K. (1999) Sea water entrainment and fluid evolution within the TAG
877 hydrothermal mound: Evidence from analyses of anhydrite. In *Mid-Ocean Ridges:*
878 *Dynamics of Processes Associated with Creation of New Ocean Crust* (ed. J. R. Cann, H.
879 Elderfield, and A. Laughton), pp. 225-248. Cambridge University Press.
880 Mitra A., Elderfield H., and Greaves M. J. (1994) Rare earth elements in submarine
881 hydrothermal fluids and plumes from the Mid-Atlantic Ridge. *Marine Chemistry* **46**(3),
882 217-235.
883 Möller P. (2002) The distribution of rare earth elements and ytttrium in water-rock interactions:
884 Field obsevations and experiments. In *Water-Rock Interaction* (ed. I. Stober and K.
885 Bucher), pp. 97-123. Kluwer Academic Publishers.
886 Paulick H. and Bach W. (2006) Phyllosilicate Alteration Mineral Assemblages in the Active
887 Subsea-Floor Pacmanus Hydrothermal System, Papua New Guinea, ODP Leg 193.
888 *Economic Geology* **101**, 633-650.
889 Paulick H., Herzig P. M., and Hoernes S. (2005) Data Report: A comprehensive geochemical,
890 mineralogical and isotopic dataset of altered dacitic volcanic rocks from the subsurface of
891 the PACMANUS hydrothemal field (ODP Leg 193). In *Proceedings of the Ocean*
892 *Drilling Program, Scientific Results*, Vol. 193 (ed. F. J. A. S. Barriga, R. A. Binns, D. J.
893 Miller, and P. M. Herzig), pp. 1-18. doi:10.2973/odp.proc.sr.193.209.2005. Ocean
894 Drilling Program.
895 Reeves E. (2010) Laboratory and field-based investigations of subsurface geochemical processes
896 in seafloor hydrothermal systems. Ph.D. Thesis, Massachusetts Institute of Technology-
897 Woods Hole Oceanographic Institution, Woods Hole, MA.
898 Roberts S., Bach W., Binns R. A., Vanko D. A., Yeats C. J., Teagle D. A. H., Blacklock K.,

899 Blusztajn J. S., Boyce A. J., and Cooper M. J. (2003) Contrasting evolution of
900 hydrothermal fluids in the PACMANUS system, Manus Basin: The Sr and S isotope
901 evidence. *Geology* **31**(9), 805-808.
902 Sakai H., Gamo T., and Scientific Crew of Cruise KH-90-3. (1991) Hydrothermal activity in the
903 eastern Manus Basin, Bismarck Sea: A brief report of the Hakuho-Maru Cruise KH-90-3.
904 *Ridge Events* **2**, 39,51.
905 Schnetzler C. C. and Philpotts J. A. (1970) Partition coefficients of rare-earth elements between
906 igneous matrix material and rock-forming mineral phenocrysts--II. *Geochimica et*
907 *Cosmochimica Acta* **34**, 331-340.
908 Seewald J. S., Doherty K. W., Hammar T. R., and Liberatore S. P. (2002) A new gas-tight
909 isobaric sampler for hydrothermal fluids. *Deep Sea Research Part I: Oceanographic*
910 *Research Papers* **49**(1), 189-196.
911 Seewald J. S., Reeves E., Saccocia P., Rouxel O. J., Walsh E., Price R. E., Tivey M., Bach W.,
912 and Tivey M. (2006) Water-rock reaction, substrate composition, magmatic degassing,
913 and mixing as major factors controlling vent fluid compositions in Manus Basin
914 hydrothermal systems. *EOS Trans. AGU. Fall Meet. Suppl.,* **87**(52), Abstract # B34A-02.
915 Sinton J. M., Ford L. L., Chappell B., and McCulloch M. T. (2003) Magma genesis and mantle
916 heterogeneity in the Manus Back-Arc Basin, Papua New Guinea. *Journal of Petrology*
917 **44**, 159-195.
918 Sun W. D., Binns R. A., Fan A. C., Kamenetsky V. S., Wysoczanski R., Wei G. J., Hu Y. H., and
919 Arculus R. J. (2007) Chlorine in submarine volcanic glasses from the eastern Manus
920 basin. *Geochimica et Cosmochimica Acta* **71**, 1542-1552.
921 Sverjensky D. A. (1984) Europium redox equilibria in aqueous solution. *Earth and Planetary*
922 *Science Letters* **67**, 70-78.
923 Taylor B. (1979) Bismarck Sea; Evolution of a back-arc basin. *Geology* **7**, 171-174.
924 Tivey M. A., Bach W., Seewald J. S., Tivey M. K., Vanko D. A., and Shipboard Science and
925 Technical Teams. (2007) Cruise Report R/V Melville, MAGELLAN-06. Hydrothermal

systems in the Eastern Manus Basin: Fluid chemistry and magnetic structures as guides to subseafloor processes, pp. 67. Woods Hole Oceanographic Institution.

Tivey M. K., Humphris S. E., Thompson G., Hannington M. D., and Rona P. A. (1995) Deducing patterns of fluid flow and mixing within the TAG active hydrothermal mound using mineralogical and geochemical data. *Journal of Geophysical Research* **100**(B7), 12527-12555.

Tivey M. K., Mills R. A., and Teagle D. A. H. (1998) Temperature and salinity of fluid inclusions in anhydrite as indicators of seawater entrainment and heating within the TAG active mound. In *Proceedings of the Ocean Drilling Program, Scientific Results*, Vol. 158 (ed. P. M. Herzig, S. E. Humphris, D. J. Miller, and R. A. Zierenberg), pp. 179-190. Ocean Drilling Program.

Tufar W. (1990) Modern hydrothermal activity, formation of complex massive sulfide deposits and associated vent communities in the Manus back-arc basin (Bismarck Sea, Papua New Guinea). *Mitteilungen der Osterreichischen Geologischen Gesellschaft* **82**, 183-210.

Von Damm K. L. (1983) Chemistry of submarine hydrothermal solutions at 21° North, East Pacific Rise and Guaymas Basin, Gulf of California. Ph. D. Thesis, Massachusetts Institute of Technology-Woods Hole Oceanographic Institution.

Von Damm K. L., Edmond J. M., Grant B., Measures C. I., Walden B., and Weiss R. F. (1985) Chemistry of submarine hydrothermal solutions at 21 °N, East Pacific Rise. *Geochimica et Cosmochimica Acta* **49**(11), 2197-2220.

Wood S. A. (1990) The aqueous geochemistry of the rare-earth elements and yttrium: 2. Theoretical predictions of speciation in hydrothermal solutions to 350 °C at saturation water vapor pressure. *Chemical Geology* **88**(1-2), 99-125.

Wood S. A. (2001) Behavior of rare earth elements in geothermal systems: A new exploration/exploitation tool? - U.S. Department of Energy Report, pp. 35. University of Idaho, Moscow, ID.

Yeats C. J., Binns R. A., and Parr J. M. (2000) Advanced argillic alteration associated with

actively forming submarine polymetallic sulfide mineralization in the eastern Manus Basin, Papua New Guinea. *Geological Society of Australia Abstracts* **59**, 555.

Fig. 1. (a) Regional tectonic setting of the Manus back-arc basin showing major plates and active plate motions (solid gray arrows). Areas of known hydrothermal activity in the Manus Spreading Center (Vienna Woods) and Eastern Manus Basin (PACMANUS, DESMOS and SuSu Knolls) are indicated by white stars; (b) Spatial distribution of known vent deposits at PACMANUS; (c) Spatial distribution of known hydrothermal deposits at SuSu Knolls. Seafloor bathymetry based on EM300 SeaBeam sonar (modified from Tivey et al., 2007).

Fig. 2. Chondrite-normalized REE distribution patterns of (a) mid-ocean ridge hydrothermal fluids and modern seawater from the Pacific and Atlantic Oceans. Data are from Michard et al. (1983), Michard (1989), Klinkhammer et al. (1994), Mitra et al. (1994) and Douville et al. (1999); (b) black/gray smoker fluids sampled from Vienna Woods, Manus Spreading Center (this study).

Fig. 3. Chondrite-normalized REE patterns of black/gray smoker fluids sampled from PACMANUS, Eastern Manus Basin. (a) Roman Ruins-Roger's Ruins; (b) Satanic Mills; (c) Fenway and (d) Snowcap and Tsukushi.

Fig. 4. Chondrite-normalized REE patterns of hydrothermal fluids sampled from DESMOS and SuSu Knolls, Eastern Manus Basin. (a) acid-sulfate fluids from DESMOS (open symbol) and North Su (filled symbol); (b) black/gray smoker fluids from North Su; (c) black/gray smoker fluids from Suzette and (d) black/gray smoker fluids from South Su.

Fig. 5. REE distribution patterns of: (a) bulk primary basalts (stippled field) and bulk primary dacites (gray field) sampled along the Manus Spreading Center (MSC) and Eastern Manus Basin (EMB). Data are from Sinton et al. (2003). Also shown are characteristic REE patterns of constituent mineral phases in mafic (basalt) and felsic (dacite, rhyolite) igneous rocks (cpx is clinopyroxene, bt is biotite, plg is plagioclase and olv is olivine). Data are from Schnetzler and Philpotts (1970). Data are normalized to average chondritic composition. (b) variably altered dacites sampled from the beneath PACMANUS, in the EMB. Solid and dashed lines indicate dacites showing incipient (chlorite-smectite) and extensive ("acid-sulfate-type", illite-pyrophyllite-alunite) alteration, respectively. Data are from Beaudoin et al. (2007) and are normalized to average chondritic composition. (c) bulk primary dacites (gray field) and highly-altered dacites ("acid-sulfate-type" alteration, shown in solid black lines) sampled at the DESMOS hydrothermal field, EMB. Data are normalized to average chondritic composition. Also shown are REE pattern of the highly-altered dacites normalized to that of the primary dacites (dashed gray lines). REE data are from Gena et al. (2001). The REE patterns of primary and altered rocks record evidence for significant and variable REE mobilization during fluid-rock interaction, similar to that inferred from the fluid REE compositions reported in this study. During low pH, acid-sulfate-type alteration, the REEs appear to be mobilized without significant fractionation among the lanthanides (c). See text for discussion.

Fig. 6. Total REE abundance versus pH for black smoker and acid-sulfate fluids sampled in the Manus Basin (this study). REE concentrations in black smoker fluids from unsedimented, mid-ocean ridge hydrothermal systems (symbol +) and in acid-sulfate fluids from continental

geothermal systems (symbol x) are shown for comparison (data from Michard, 1989; Klinkhammer et al., 1994; Lewis et al., 1997; Douville et al., 1999). Smoker-type fluids with lower temperatures (< 280 °C) and elevated Mg concentrations (> 10 mmol/kg) are not plotted as these fluids have experienced local sub-seafloor mixing with seawater and the measured pH (25 °C) of these fluids does not reflect that of the high-temperature hydrothermal fluid at depth.

Fig. 7. Correlations between aqueous [ΣF]/[ΣCl] ratios and chondrite-normalized La_N/Yb_N (a) and Eu_N/Eu^*_N ratios (b) in black smoker and acid-sulfate fluids from the Manus Basin. Data for all vent areas are grouped by measured pH (25 °C). Smoker fluids with lower temperatures (< 280 °C) and elevated Mg concentrations (> 10 mmol/kg) are not plotted. Smoker fluids (pH > 2 to 4) show decreasing La_N/Yb_N and Eu_N/Eu^*_N ratios (increasing heavy-REE abundances relative to light-REEs and Eu) with increasing [ΣF]/[ΣCl] ratios. Acid-sulfate fluids (pH < 2) show no clear differences in La_N/Yb_N and Eu_N/Eu^*_N ratios for a wide range of [ΣF]/ΣCl] ratios. Differences in ligand abundances affect aqueous REE_N distributions likely owing to the formation of various REE-ligand complexes with different stabilities. See text for discussion.

Fig. 8. Predicted REE species distributions in high-temperature smoker fluids from the Manus Basin. (a) fluid VW1 (Vienna Woods); (b) fluid RMR4 (Roman Ruins, PACMANUS); (c) fluid SM1 (Satanic Mills, PACMANUS); (d) fluid SM2 (Satanic Mills, PACMANUS); (e) fluid SZ5 (Suzette, SuSu Knolls); (f) fluid NS2 (North Su, SuSu Knolls) and (g) fluid D1 (DESMOS). REE-chloride, REE-fluoride and REE-sulfate complexes are shown by black

squares, white triangles and gray diamonds, respectively. REE-oxyhydroxide complexes are shown by gray circles and free REE ions by black crosses. Fluid compositions used in calculations are reported in Tables 1 and 3.

Fig. 9. Fractional abundance of (a) fluoride present in solution as HF and Al-fluoride complexes and (b) REE present in solution as REE-fluoride complexes, versus measured fluid pH (25 °C) for hydrothermal fluids listed in Table 3. The dashed line in (a) is the modeled fractional abundance of HF relative to total fluoride in the absence of Al-fluoride complexation (i.e., Al^{3+} removed from fluid compositions for species distribution calculations). The values in parentheses in (b) are measured fluoride concentrations. At low pH in acid-sulfate fluids, fluoride is effectively bound as HF and is unavailable to complex REEs. The presence or absence of Al-fluoride complexes does not affect predicted REE-fluoride complex abundances (dashed line follows modeled fluids). At higher pH in smoker fluids, proportionally more fluoride is dissociated and available to complex with REEs. The fraction of REE complexed with fluoride is significant in fluoride-rich (≥ 400 μM) hydrothermal fluids at pH > 2.

Fig. 10. Compositions of black/gray smoker fluids from PACMANUS. (a) sulfate versus Mg; (b) chloride-normalized Ca versus Mg; (c) chloride-normalized end-member Ca versus end-member sulfate; and (d) chloride-normalized end-member REE versus end-member sulfate. Symbols as follows: Roman Ruins – gray diamonds, Satanic Mills – black triangles, Fenway – light-gray squares, Snowcap – open circles. The composition of ambient seawater is shown by the star. Normalization of calcium to chloride removes differences in Ca concentrations

among hydrothermal fluids from individual vent areas resulting from sub-seafloor phase separation. Conservative mixing lines between end-member (zero Mg, zero sulfate) hydrothermal fluid (>> 300 °C) and seawater are shown by the black dashed lines in each plot. Many lower temperature (< 280 °C) vent fluids have measurable Mg and sulfate owing to local entrainment and sub-seafloor mixing of seawater with end-member hydrothermal fluid (a). Measured sulfate, Ca and REE concentrations in many lower temperature fluids are, however, less than that predicted by conservative mixing owing to removal during anhydrite ($CaSO_4$) precipitation (fluids SC1, SC2, RMR2, SM2). The extent of anhydrite precipitation is indicated by the magnitude of the negative sulfate end-member anomaly. In contrast, low temperature fluids from Fenway (fluid F5) show excess sulfate, Ca and REE concentrations relative to those predicted by conservative mixing, suggesting current dissolution of previously deposited anhydrite in the Fenway mound.

Table 1. Rare earth element concentrations (pmol/kg) in sampled smoker- and acid-sulfate-type fluids from the Manus Basin. Data are reported at the lowest measured Mg.

Sample	Vent Site	Temp (°C)	pH (25 °C)	Mg (mM)	La	Ce	Pr	Nd	Sm	Eu	Gd	Tb	Dy	Ho	Er	Yb	ΣF/ΣCl (x1000)	$\Sigma SO_4/\Sigma Cl$ (x1000)	ΣCa/ΣCl
Smoker Fluids																			
VW1	Vienna Woods	282	4.4	1.4	1700	1750	180	532	88	738	81	14	43	14	30	21	0.03	0.9	0.116
VW2	Vienna Woods	273	4.2	1.0	1021	1244	157	467	81	629	61	10	33	14	25	19	0.03	0.6	0.117
VW3	Vienna Woods	285	4.7	1.1	740	958	110	291	45	390	32	7	20	19	19	11	0.03	1.5	0.105
RMR1	Roman Ruins	314	2.3	7.3	8493	10417	837	2225	520	6848	187	27	132	21	57	65	0.19	1.6	0.030
RMR2	Roman Ruins	272	2.3	15.9	979	2210	283	1134	278	2865	188	27	207	22	59	59	0.17	5.5	0.019
RMR3	Roman Ruins	278	2.5	6.4	9585	15412	1935	7369	1568	16075	1121	134	626	86	221	170	0.22	2.5	0.034
RMR4	Roman Ruins	341	2.6	3.6	12500	22500	2830	10213	2075	11182	1324	154	685	97	228	191	0.19	1.7	0.034
RGR1	Roger's Ruins	320	2.7	4.2	6500	11332	1416	5926	1389	7698	959	102	438	55	135	85	0.23	2.7	0.040
RGR2	Roger's Ruins	274	2.6	8.6	1165	2225	230	868	250	1712	232	28	135	18	42	45	0.21	3.0	0.035
SM1	Satanic Mills	295	2.6	8.2	1361	3326	480	2179	685	3417	545	73	357	59	143	120	0.29	3.7	0.022
SM2	Satanic Mills	241	2.4	16.9	330	800	125	694	389	677	1583	395	2777	479	1307	965	0.63	15.6	0.013
SM3	Satanic Mills	288	2.5	9.7	1078	2481	410	2137	1050	2477	1705	258	1362	221	593	443	0.40	5.3	0.026
SC1	Snowcap	152	4.6	30.8	221	411	46	176	83	105	58	16	112	26	83	70	0.26	22.8	0.013
SC2	Snowcap	180	3.4	24.2	352	827	70	284	56	140	50	12	70	16	40	40	0.32	10.3	0.013
TK1	Tsukushi	62	5.7	44.4	309	661	73	293	80	185	70	17	95	28	75	55	0.13	38.5	0.022
F1	Fenway	329	2.5	5.8	859	1971	232	1252	1868	7362	2073	283	1338	203	530	401	0.61	4.3	0.031
F2	Fenway	343	2.7	4.7	19716	33980	3982	14465	2851	8514	1979	250	1210	165	405	314	0.25	2.5	0.038
F3	Fenway	358	2.7	4.5	15000	27172	3400	14000	3400	7750	2750	320	1500	205	470	290	0.29	3.9	0.039
F4	Fenway	284	2.4	8.9	3000	9130	1200	5260	1610	5060	1970	430	3100	385	1150	900	0.30	5.9	0.034
F5	Fenway	78	5.0	44.7	1960	4700	560	2070	520	1075	655	110	760	nd	210	100	0.16	52.6	0.026
SZ1	Suzette	303	3.8	4.4	3478	5736	726	2607	444	2741	291	32	163	25	65	61	0.10	2.3	0.051
SZ2	Suzette	274	3.6	8.6	3095	5250	624	2450	546	2701	373	41	192	27	76	66	0.12	2.9	0.066
SZ3	Suzette	290	3.5	5.5	3035	6237	950	4652	1300	4798	841	88	347	49	110	83	0.12	1.5	0.066
SZ4	Suzette	229	3.6	8.3	868	1767	256	1150	279	1607	214	31	125	42	53	41	0.10	2.4	0.059
SZ5	Suzette	249	2.3	6.4	2400	4094	668	3979	2561	1304	4005	739	4637	864	2486	2076	0.79	6.7	0.040
SZ6	Suzette	226	3.7	8.0	2322	4120	594	2549	606	5024	459	45	192	26	60	54	0.12	1.9	0.066
NS3	North Su	300	3.4	1.6	10689	18408	2075	6913	840	3089	424	41	179	29	66	60	0.21	1.1	0.046
NS5	North Su	299	3.2	7.4	836	1700	330	2031	752	2341	265	20	90	16	37	51	0.31	4.2	0.034
NS6	North Su	325	2.8	1.6	590	690	99	470	282	1502	399	59	318	54	142	147	0.48	1.4	0.052
SS1	South Su	271	2.6	5.3	536	1250	126	452	201	181	212	57	521	91	235	164	0.56	3.3	0.045
SS2	South Su	288	2.7	6.8	480	681	70	207	61	621	51	13	62	16	47	58	0.43	3.2	0.042
Acid-Sulfate Fluids																			
D1	DESMOS	117	1.0	46.0	17862	54166	7331	31845	7830	2948	7283	1160	6980	1330	4044	3826	0.28	297.5	0.019
D2	DESMOS	70	1.4	50.4	20805	71826	11431	55550	15736	6526	14321	2267	13865	2595	7773	7336	0.01	123.7	0.024
NS1	North Su	48	1.8	49.0	10923	35507	4755	19616	4699	1782	4452	718	4452	876	2793	2846	0.09	78.5	0.018
NS2	North Su	215	0.9	38.8	25597	98058	16244	83537	25511	8865	26764	4323	26644	5155	15724	15225	0.23	335.5	0.020
NS4	North Su	241	1.5	23.5	12657	47812	6540	29310	9834	3549	13534	2355	15301	3064	9287	8503	0.94	48.0	0.012

Table 2. Endmember (zero Mg) rare earth element concentrations (pmol/kg) in smoker fluids sampled in the Manus Basin.

Sample	Vent Site	Temp (°C)	pH (25 °C)	La	Ce	Pr	Nd	Sm	Eu	Gd	Tb	Dy	Ho	Er	Yb
VW1	Vienna Woods	282	4.4	1700	1750	180	532	88	738	81	14	43	14	30	21
VW2	Vienna Woods	273	4.2	1021	1244	157	467	81	629	61	10	33	14	25	19
VW3	Vienna Woods	285	4.7	740	958	110	291	45	390	32	7	20	19	19	11
RMR1	Roman Ruins	314	2.3	9918	12164	977	2599	607	7996	219	31	154	24	67	76
RMR2	Roman Ruins	272	2.3	1392	3140	402	1612	395	4072	268	39	294	32	83	84
RMR3	Roman Ruins	278	2.5	10829	17413	2186	8326	1772	18162	1267	151	708	98	249	192
RMR4	Roman Ruins	341	2.6	13262	23871	3002	10835	2201	11863	1405	164	727	103	242	202
RGR1	Roger's Ruins	320	2.7	7071	12328	1540	6447	1511	8374	1044	111	476	60	147	92
RGR2	Roger's Ruins	274	2.6	1390	2653	274	1035	299	2042	277	34	161	21	51	53
SM1	Satanic Mills	295	2.6	1617	3950	570	2588	813	4058	647	87	424	69	170	143
SM2	Satanic Mills	241	2.4	480	1163	182	1009	566	984	2303	575	4039	697	1901	1404
SM3	Satanic Mills	288	2.5	1317	3031	501	2612	1283	3027	2084	315	1664	270	725	541
SC1	Snowcap	152	4.6	499	928	103	396	186	237	130	35	251	58	188	158
SC2	Snowcap	180	3.4	619	1454	123	500	99	246	88	21	123	28	70	70
TK1	Tsukushi	62	5.7	1470	3148	349	1397	379	881	335	81	452	135	357	262
F1	Fenway	329	2.5	959	2200	259	1397	2085	8217	2313	315	1493	226	592	448
F2	Fenway	343	2.7	21528	37103	4348	15794	3113	9296	2161	273	1321	180	442	343
F3	Fenway	358	2.7	16318	29560	3699	15230	3699	8431	2992	348	1632	223	511	315
F4	Fenway	284	2.4	3609	10984	1444	6328	1937	6087	2370	517	3729	463	1383	1083
F5	Fenway	78	5.0	9925	23799	2836	10482	2633	5443	3317	557	3848	nd	1063	506
SZ1	Suzette	303	3.8	3777	6228	788	2831	482	2976	316	35	177	27	70	67
SZ2	Suzette	274	3.6	3660	6209	738	2897	646	3194	441	48	227	32	90	78
SZ3	Suzette	290	3.5	3368	6921	1054	5162	1442	5324	933	97	386	55	122	92
SZ4	Suzette	229	3.6	1020	2077	301	1352	327	1888	251	36	147	50	63	48
SZ5	Suzette	249	2.3	2711	4625	755	4495	2893	1473	4525	834	5239	976	2808	2345
SZ6	Suzette	226	3.7	2711	4811	693	2976	708	5866	536	52	225	30	70	63
NS3	North Su	300	3.4	10689	18408	2075	6913	840	3089	424	41	179	29	66	60
NS5	North Su	299	3.2	964	1960	380	2342	867	2700	306	23	104	18	43	58
NS6	North Su	325	2.8	590	690	99	470	282	1502	399	59	318	54	142	147
SS1	South Su	271	2.6	592	1381	139	499	222	201	234	63	576	101	260	181
SS2	South Su	288	2.7	547	775	80	236	69	708	58	15	71	18	53	66

Table 3. Chemical compositions of representative hydrothermal fluids used in thermodynamic REE speciation calculations.

Sample	Vent Site	Temp (°C)	pH (25°C)	pH (in situ)	Mg (mmol/kg)	Cl (mmol/kg)	Na (mmol/kg)	K (mmol/kg)	Ca (mmol/kg)	Ba (µmol/kg)	Al (µmol/kg)	Mn (µmol/kg)	Fe (µmol/kg)	SiO_2 (mmol/kg)	SO_4 (mmol/kg)	F (µmol/kg)	CO_2 (mmol/kg)	H_2S (mmol/kg)	H_2 (µmol/kg)
Smoker Fluids																			
VW1	Vienna Woods	282	4.4	4.8	1.4	690	512	21.2	80.0	55	< 10	349	159	15.3	0.8	21	4.4	1.4	42
RMR4	Roman Ruins	341	2.6	3.37	3.6	650	495	77.2	22.3	92	< 10	2830	6468	17.8	0.4	125	9.5	6.3	53
SM1	Satanic Mills	295	2.6	3.25	8.2	519	407	60.5	12.5	20	< 10	2145	2790	12.2	2.1	167	181	8.0	25
SM2	Satanic Mills	241	2.4	3.2	16.9	455	374	38.6	5.9	16	< 10	1853	1045	12.8	7.1	287	112	4.5	4.3
SZ5	Suzette	249	2.3	2.7	6.4	610	493	44.3	24.2	16	18	243	3961	14.1	3.0	480	16.1	4.8	7.4
Acid-Sulfate Fluids																			
D1	DESMOS	117	1.0	1.2	46.0	492	391	8.3	9.4	< 1	480	40	12400	8.1	147	137	23.1	0.0	4.0
NS2	North Su	215	0.9	1.18	38.8	442	340	7.8	8.9	nd	1075	81	3103	10.0	149	128	80.0	0.0	20

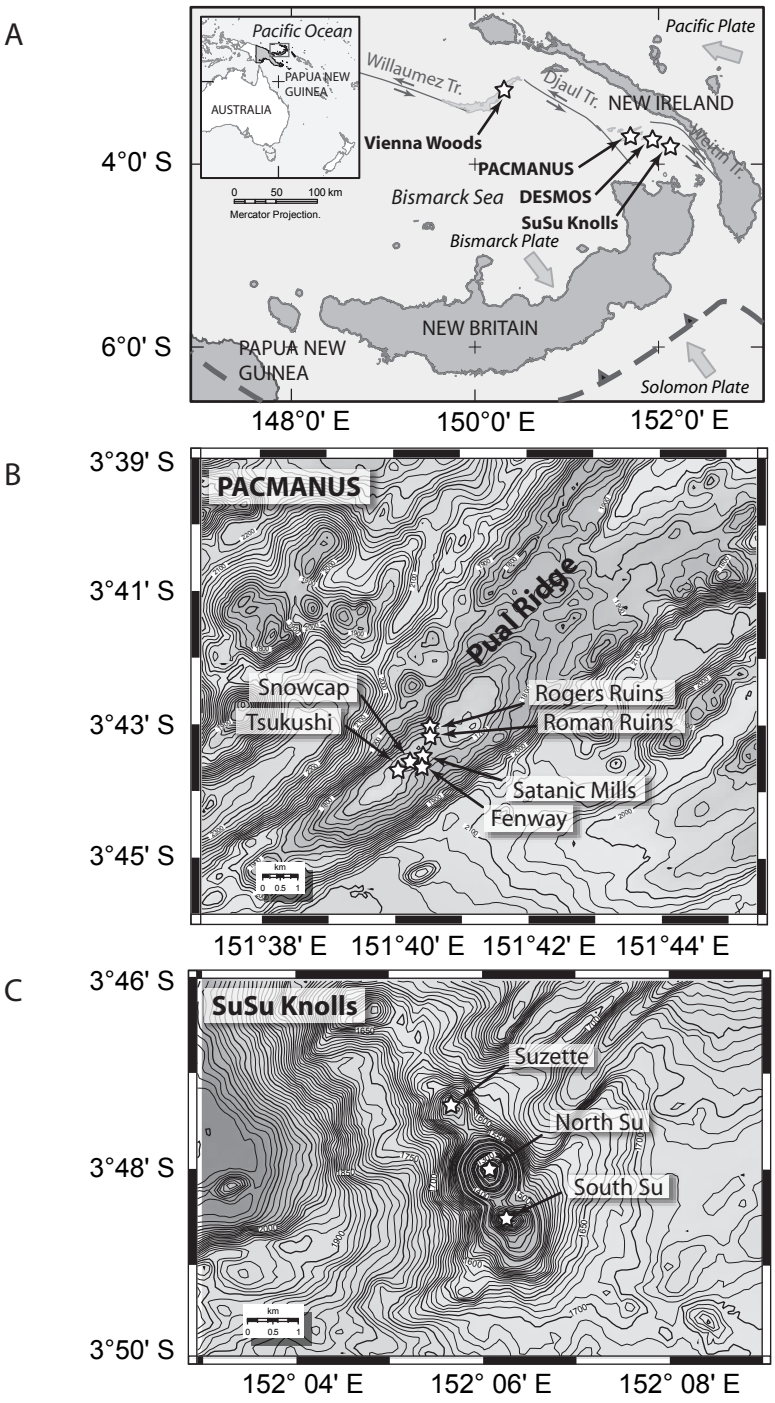
A
Pacific Ocean
PAPUA NEW GUINEA
AUSTRALIA
0 50 100 km
Mercator Projection.
Willaumez Tr.
Djaul Tr.
Pacific Plate
NEW IRELAND
Weitin Tr.
Vienna Woods
PACMANUS
DESMOS
SuSu Knolls
Bismarck Sea
Bismarck Plate
NEW BRITAIN
PAPUA NEW GUINEA
Solomon Plate
4°0' S
6°0' S
148°0' E
150°0' E
152°0' E
B
PACMANUS
Pual Ridge
Snowcap
Tsukushi
Rogers Ruins
Roman Ruins
Satanic Mills
Fenway
3°39' S
3°41' S
3°43' S
3°45' S
151°38' E
151°40' E
151°42' E
151°44' E
C
SuSu Knolls
Suzette
North Su
South Su
3°46' S
3°48' S
3°50' S
152° 04' E
152° 06' E
152° 08' E

Fig. 1

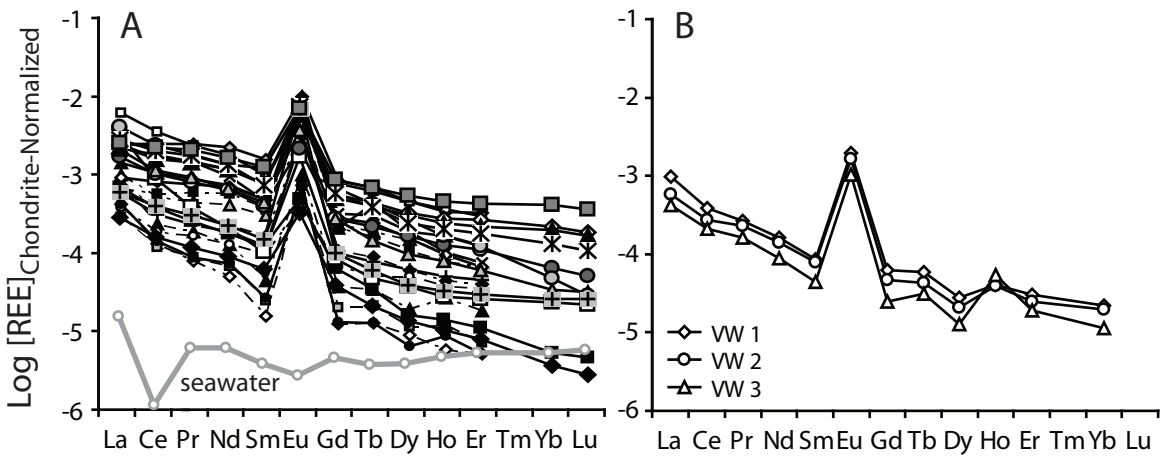
A
B
Log [REE]Chondrite-Normalized
-1
-2
-3
-4
-5
-6
seawater
VW 1
VW 2
VW 3
La Ce Pr Nd Sm Eu Gd Tb Dy Ho Er Tm Yb Lu

Fig. 2

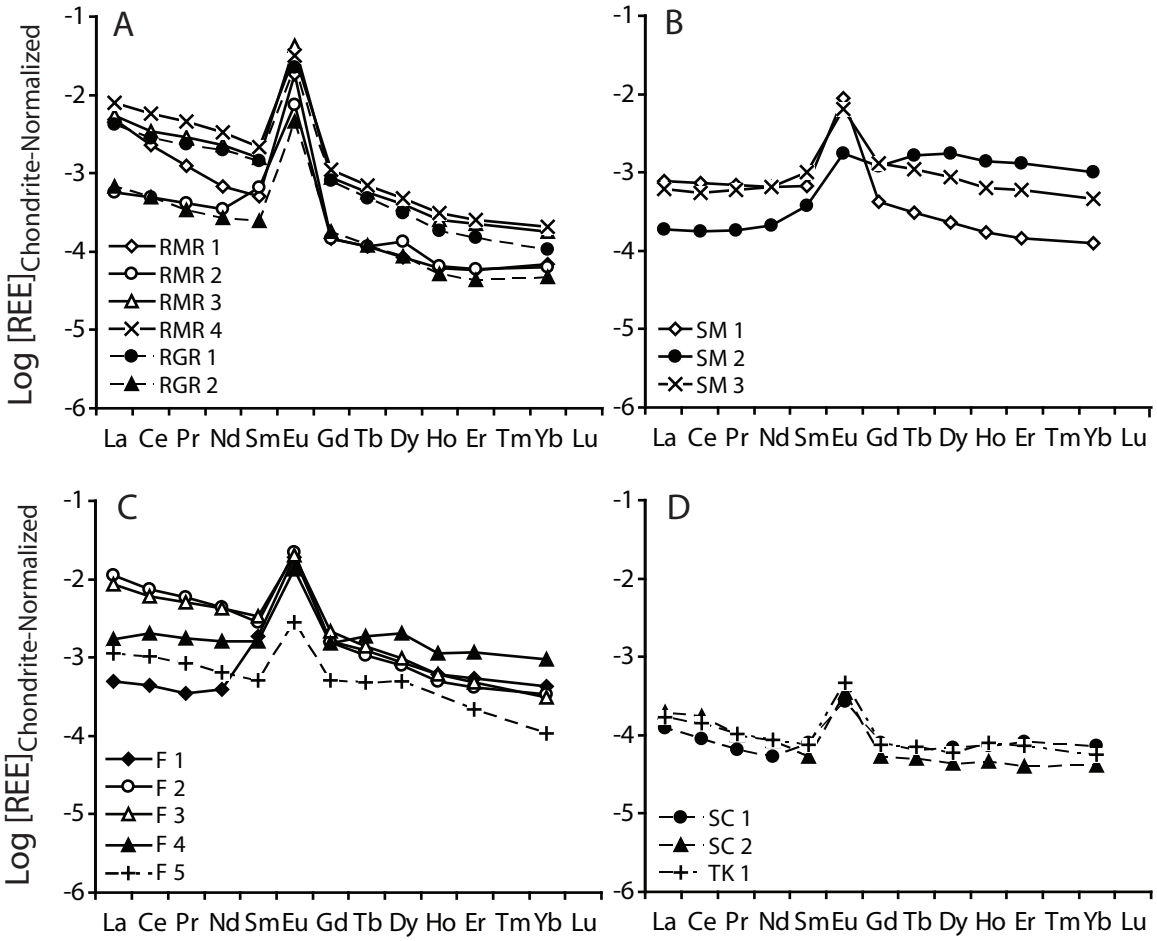
A
B
C
D
Log [REE]Chondrite-Normalized
-1
-2
-3
-4
-5
-6
La Ce Pr Nd Sm Eu Gd Tb Dy Ho Er Tm Yb Lu
RMR 1
RMR 2
RMR 3
RMR 4
RGR 1
RGR 2
SM 1
SM 2
SM 3
F 1
F 2
F 3
F 4
F 5
SC 1
SC 2
TK 1

Fig. 3

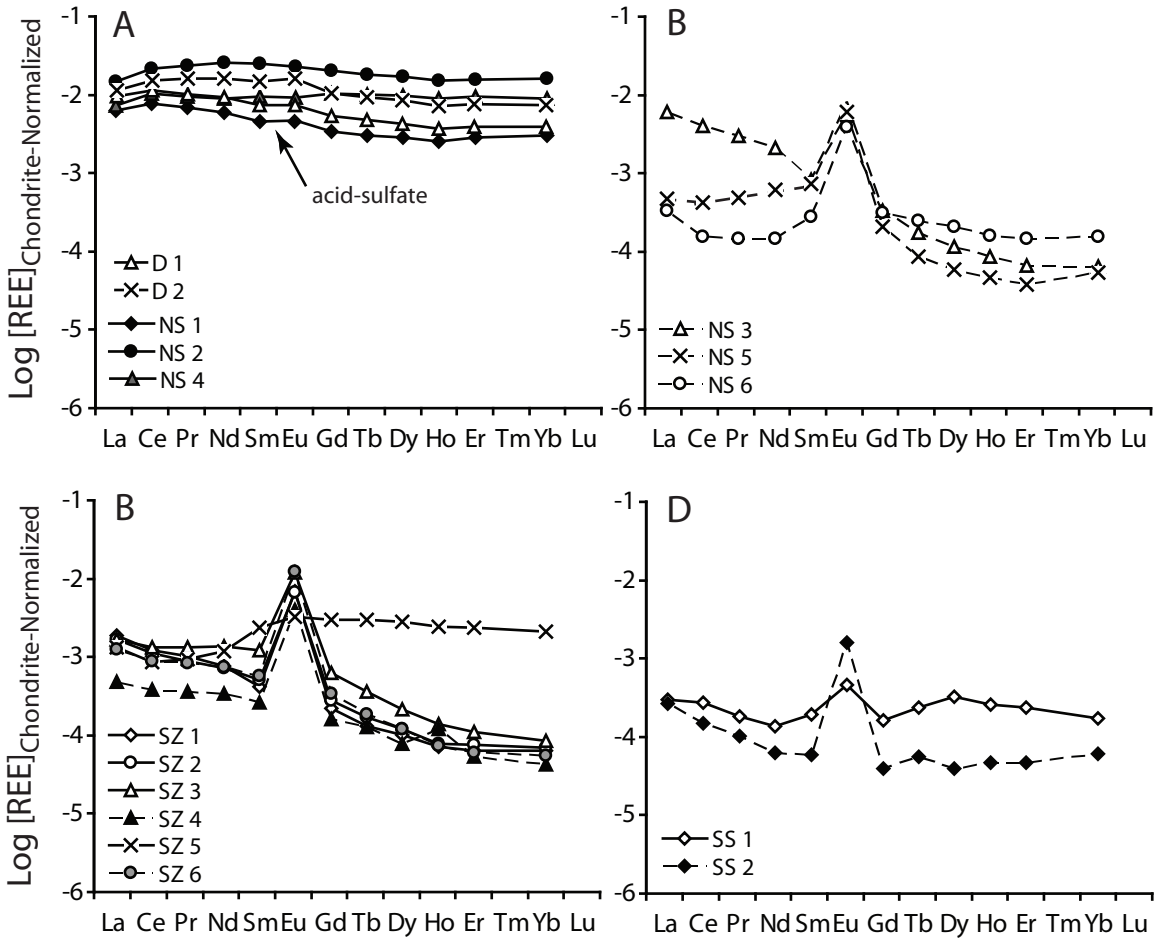
A
B
B
D
Log [REE]Chondrite-Normalized
-1
-2
-3
-4
-5
-6
La Ce Pr Nd Sm Eu Gd Tb Dy Ho Er Tm Yb Lu
acid-sulfate
D 1
D 2
NS 1
NS 2
NS 4
NS 3
NS 5
NS 6
SZ 1
SZ 2
SZ 3
SZ 4
SZ 5
SZ 6
SS 1
SS 2

Fig. 4

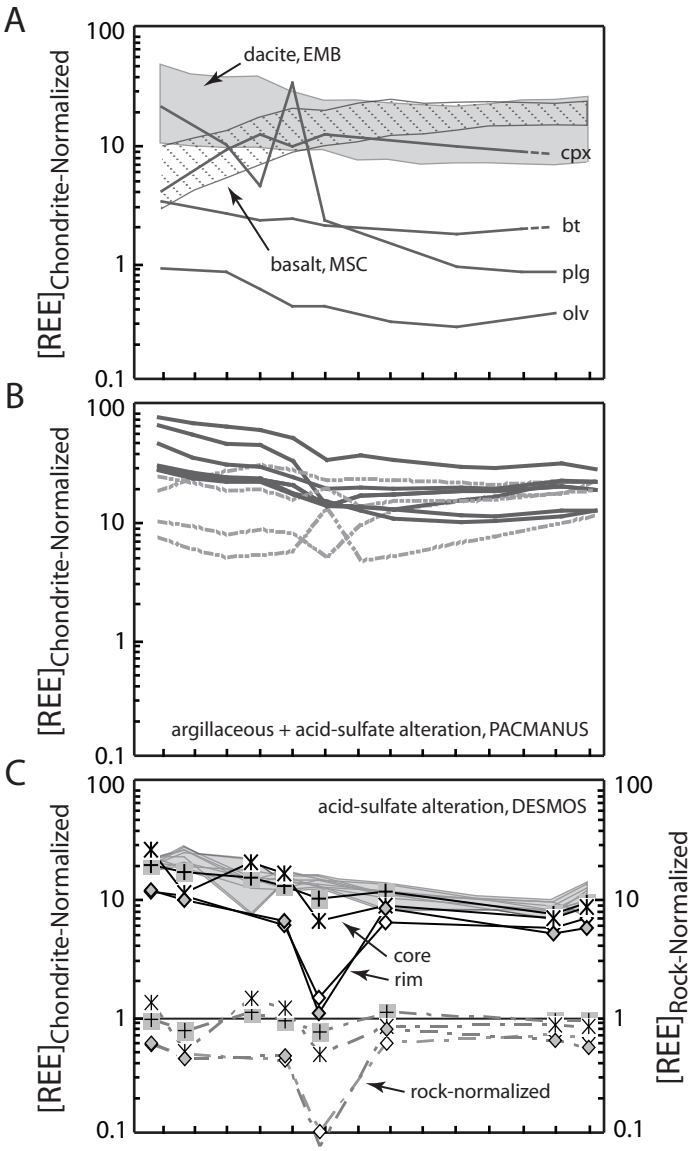
A
100
10
1
0.1
[REE]Chondrite-Normalized
dacite, EMB
cpx
bt
basalt, MSC
plg
olv
B
argillaceous + acid-sulfate alteration, PACMANUS
C
acid-sulfate alteration, DESMOS
core
rim
rock-normalized
[REE]Rock-Normalized

Fig. 5

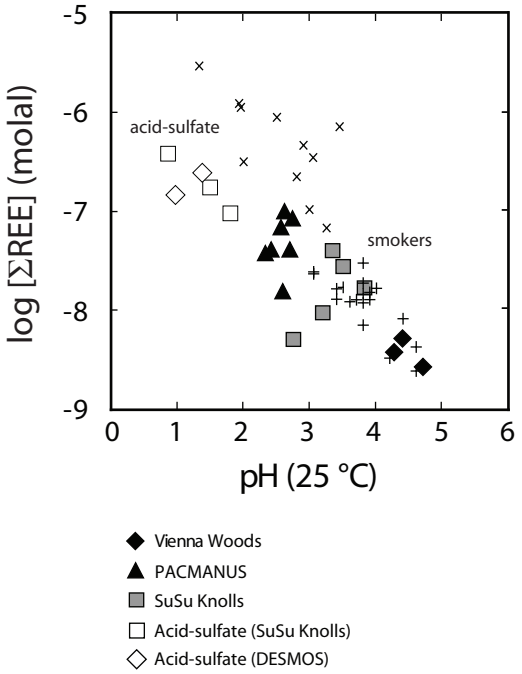
log [ΣREE] (molal)
-5
-6
-7
-8
-9
0
1
2
3
4
5
6
pH (25 °C)
acid-sulfate
smokers
Vienna Woods
PACMANUS
SuSu Knolls
Acid-sulfate (SuSu Knolls)
Acid-sulfate (DESMOS)

Fig. 6

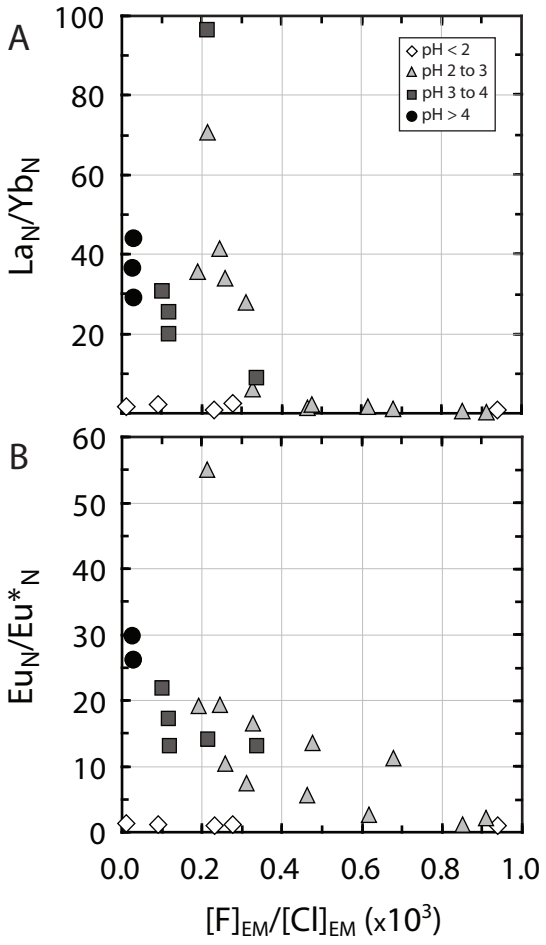
A
B
pH < 2
pH 2 to 3
pH 3 to 4
pH > 4
La_N/Yb_N
Eu_N/Eu*_N
[F]_EM/[Cl]_EM (x10^3)
0
20
40
60
80
100
10
30
50
0.0
0.2
0.4
0.6
0.8
1.0

Fig. 7

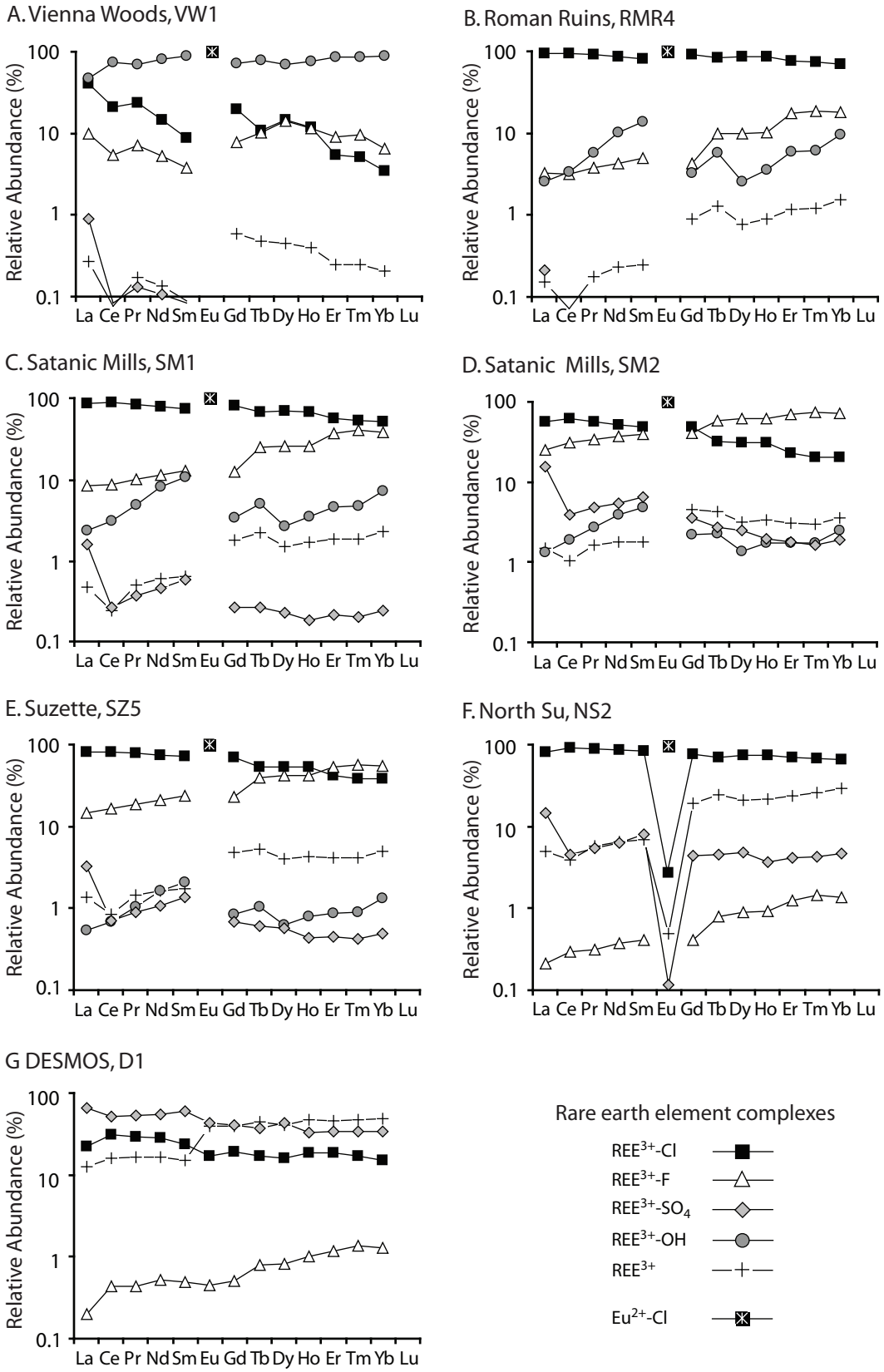
A. Vienna Woods, VW1
B. Roman Ruins, RMR4
C. Satanic Mills, SM1
D. Satanic Mills, SM2
E. Suzette, SZ5
F. North Su, NS2
G DESMOS, D1
Relative Abundance (%)
100
10
1
0.1
La Ce Pr Nd Sm Eu Gd Tb Dy Ho Er Tm Yb Lu
Rare earth element complexes
REE3+-Cl
REE3+-F
REE3+-SO4
REE3+-OH
REE3+
Eu2+-Cl

Fig. 8

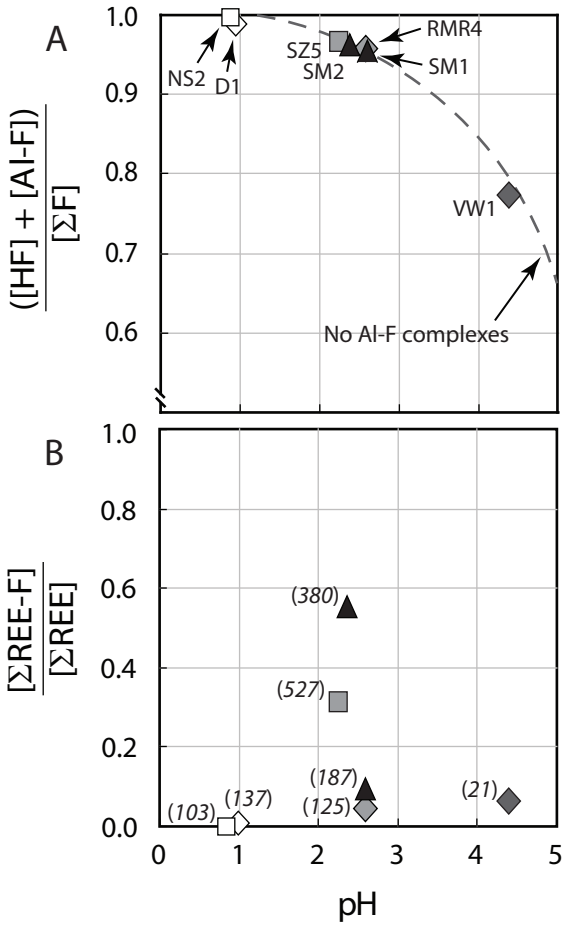
A
B
([HF] + [Al-F])
[ΣF]
[ΣREE-F]
[ΣREE]
NS2
D1
SZ5
SM2
RMR4
SM1
VW1
No Al-F complexes
(380)
(527)
(187)
(125)
(21)
(137)
(103)
pH
1.0
0.9
0.8
0.7
0.6
0.4
0.2
0.0
0
1
2
3
4
5

Fig. 9

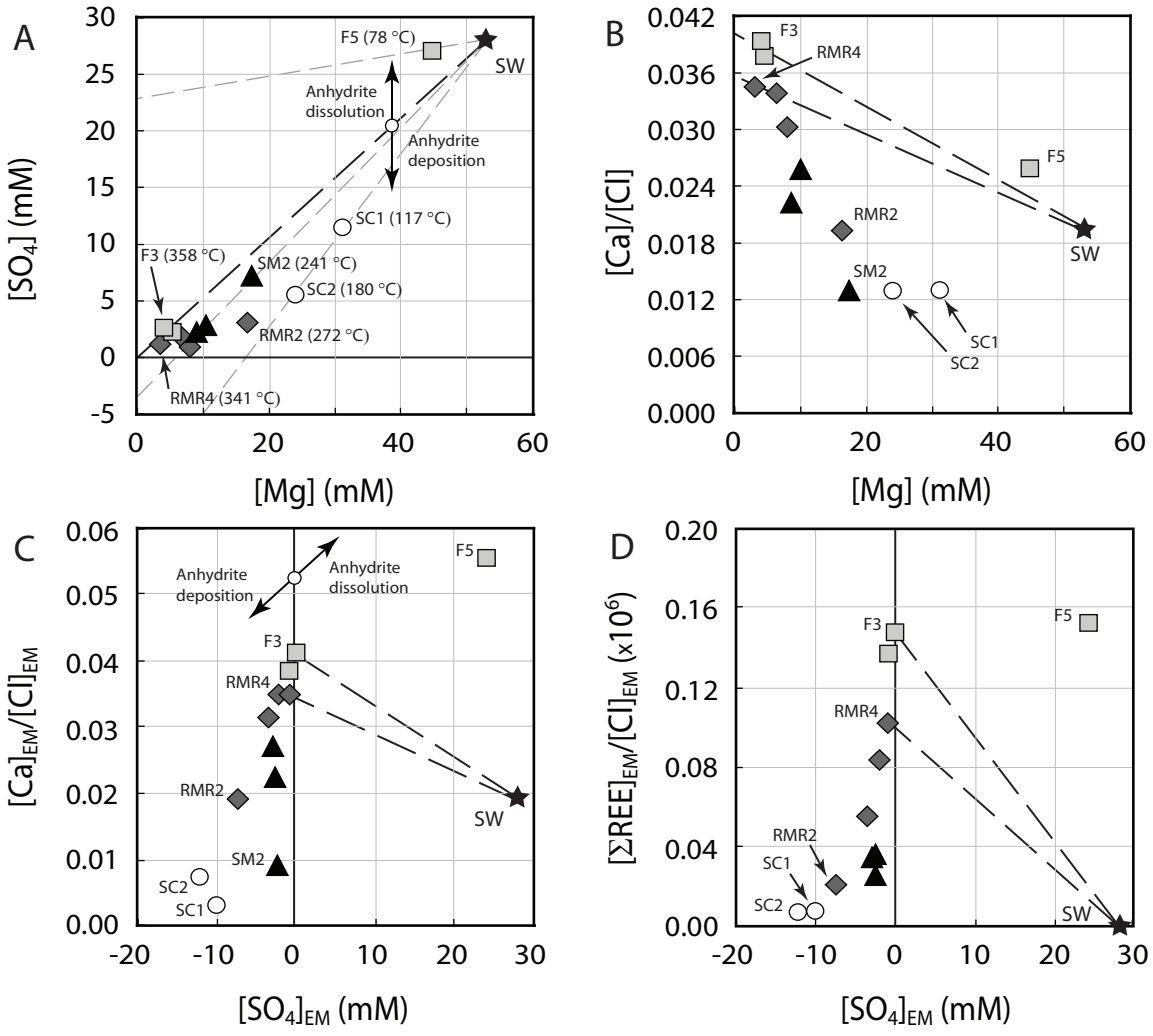
A
[SO4] (mM)
[Mg] (mM)
F5 (78 °C)
SW
Anhydrite dissolution
Anhydrite deposition
SC1 (117 °C)
F3 (358 °C)
SM2 (241 °C)
SC2 (180 °C)
RMR2 (272 °C)
RMR4 (341 °C)
B
[Ca]/[Cl]
[Mg] (mM)
F3
RMR4
F5
RMR2
SW
SM2
SC1
SC2
C
[Ca]EM/[Cl]EM
[SO4]EM (mM)
Anhydrite deposition
Anhydrite dissolution
F5
F3
RMR4
RMR2
SW
SM2
SC2
SC1
D
[ΣREE]EM/[Cl]EM (x10^6)
[SO4]EM (mM)
F3
F5
RMR4
RMR2
SC1
SC2
SW

Fig. 10

Supporting Online Material.

to accompany Craddock *et al*. Rare Earth Element Abundances in Hydrothermal Fluids from the Manus Basin, Papua New Guinea: Indicators of Sub-seafloor Hydrothermal Processes in Back-Arc Basins

Information about thermodynamic calculations used in this study

Rare earth element (REE) species distribution calculations were carried out using the SpecE8 program, included as a module of the Geochemist's Workbench (v6.0) software package (Bethke, 1996). The SpecE8 program computes species distributions, mineral saturation states and gas fugacity in aqueous solutions at specified temperature and pressure. The objectives of our calculations are to assess whether differences in composition (e.g., Cl^-, F^- and SO_4^{2-} concentration, pH) among sampled vent fluids result in significantly different REE species distributions that might be consistent with and responsible for the observed differences in REE concentrations and REE_N distribution patterns. Our calculations do not predict the absolute abundance or solubility of REEs in these fluids as thermodynamic data for REE mineral solubility and fluid-mineral partitioning are not available.

The thermodynamic database used in SpecE8 calculations was generated using the SUPCRT92 program (Johnson et al., 1992) for a pressure of 50 MPa (500 bars) and temperatures between 0 and 400 °C. Our SUPCRT92 database includes updates to and addition of to inorganic aqueous species formation constants current to November 2007 that are included in the SUPCRT92 compatible data file OBIGT.dat (see OrganoBIoGeoTherm documentation available at http://pdukonline.co.uk/download/obigt/sources). All aqueous species for which thermodynamic properties were considered in these calculations are listed in this SOM. The following compositional parameters (all major and relevant accessory species) were used in the speciation calculations: concentrations of Na^+, K^+, Ca^{2+}, Mg^{2+}, Ba^{2+},

Fe^{2+}, Mn^{2+}, Al^{3+}, all REEs, Cl^-, F^-, SO_4^{2-}, SiO_2(aq), H_2S(aq), H_2(aq), and total CO_2. Inclusion of full fluid compositions enabled us to examine competition between the REE and other cations to form complexes with available ligands. For example, inclusion of thermodynamic data for Al–fluoride complexes (Tagirov and Schott, 2001) enabled us to examine competition between Al^{3+} and REE^{3+} to form complexes with fluoride (c.f. Gimeno Serrano et al., 2000). The pH value of each fluid measured at 25 °C was used together with aqueous compositional data to calculate pH at in situ temperature. The extended Debye–Hückel equation was used to calculate activity coefficients with extended parameters (β-gamma) and hard core diameters for each species from Wolery (2003). Dissolved neutral species were assigned an activity coefficient of one (Helgeson, 1969). In all calculations, mineral precipitation and redox reactions between species were suppressed. Exceptions were reactions between H_2/H_2O, Fe^{3+}/Fe^{2+}, Mn^{3+}/Mn^{2+}, and Eu^{3+}/Eu^{2+}. The redox potential for each fluid was calculated based on measured H_2(aq) concentrations and the assumption of H_2(aq)-H_2O equilibrium. Equilibrium between valency states of redox-sensitive elements was allowed in order to examine the effects of differences in temperature and fO_2 on the oxidation state and resulting speciation of these elements. Equilibrium between H_2S and SO_4^{2-} was suppressed because both species were measured in our hydrothermal fluids and are in a state of non-equilibrium. Suppression of mineral precipitation reflects that our calculations are used to predict species distributions of real fluid compositions at in situ temperature in the absence of mineral precipitation.

In this paper, the theoretically-determined formation constants for REE complexes provided by Haas et al. (1995) are used in species distribution calculations. These theoretical data are not without uncertainty, and for some REE-complexes are not in agreement with

formation constants estimated independently from experimental studies. For example, it has been suggested on the basis of experimental data for Nd speciation in Cl-rich fluids that theoretical constants over-predict the stability of Nd (and other REE) hydroxide complexes (e.g., Gammons et al., 1996; Wood et al., 2002). If this is correct, REE speciation in hydrothermal fluids would be more dominated by REE-chloride complexes than our calculations predict. Most recently, a systematic experimental endeavor has been undertaken to characterize the solubility and speciation of all REEs in aqueous solutions at elevated temperatures with a wide range of chloride- fluoride- and sulfate compositions (e.g., Migdisov et al., 2006; Migdisov and Williams-Jones, 2006, 2007, 2008; Migdisov et al., 2008; Migdisov et al., 2009). The agreement between the theoretically predicted REE formation constants of Haas et al. (1995) and those determined experimentally by Migdisov and co-workers varies. There is relatively good agreement between theoretically and experimentally determined first and second formation constants of REE-chloride complexes ($REECl^{2+}$ and $REECl_2^{+}$), in particular for the heavy REEs. Experimental studies suggest that the stability chloride complexes of the light REEs are, however, moderately under predicted by theoretical calculations of Haas et al. (1995). No experimental data are available for higher order chloride complexes (i.e., $REECl_3^{0}$(aq) and $REECl_4^{-}$). There is good agreement between the first and second formation constants of REE-sulfate complexes ($REESO_4^{+}$ and $REE(SO_4)_2^{-}$) determined theoretically and experimentally (Migdisov and Williams-Jones, 2008). It is critical to note, however, that experimentally-derived formation constants are available only for three REE (Nd, Sm and Er), and so it is not possible to compare theoretically and experimentally derived formation constants for all REE-sulfate complexes, nor is it possible to consider experimentally determined REE-sulfate thermodynamic data in our calculations.

The theoretically (Haas et al., 1995) and experimentally determined (Migdisov et al., 2009) formation constants of REE-fluoride complexes show considerable discrepancies. For all REEs, the stability of REE-fluoride complexes derived experimentally is significantly lower than that predicted from theoretical calculations. Experimental data suggest that the stability of the heavy-REE fluoride complexes is strongly over-predicted by theoretical calculations and, at elevated temperatures (≥ 250 °C), the stability of heavy-REE fluoride complexes is not greater than that of light-REE fluorides.

The choice of thermodynamic data used will have a small affect on the results of our REE species distribution calculations. For example, the use of experimentally-derived thermodynamic data by Migdisov and co-workers would predict a lower relative abundance of REE-fluoride complexes relative to that of REE-chloride complexes (in particular for the heavy-REEs) within all hydrothermal fluids. The results of Migdisov et al. (2009) would imply that the importance of REE-fluoride complexing (i.e., absolute abundance of REE-fluoride complexes) in high temperature hydrothermal fluids is over-stated. However, it is important to note that our calculations are used only to identify relative differences in the species distribution of the REEs *between* fluids of different composition. Relative differences in the REE species distribution predicted between fluids are robust in all instances and do not impact our interpretation of the calculations. Clearly, it would be most instructive to model and compare REE species distributions in seafloor hydrothermal fluids using both theoretically- and experimentally-derived REE thermodynamic data. However, a fully inclusive and internally consistent experimental database is not yet available, notably for REE-sulfate, (oxy)hydroxide and carbonate complexes, which would enable such a

comparison with theoretical predictions. In the absence of a complete experimentally-derived REE thermodynamic database, we rely on the theoretical predictions of Haas et al. (1995).

List of aqueous species considered in thermodynamic calculations

Al^{+3}	(TS01)	$EuCl_n^{+3-n}$	(HSS95)
$Al(OH)_n^{+3-n}$	(TS01), (SSW97)	EuF_n^{+2-n}	(HSS95)
$Al(OH)_nF_{3-n}^{+3-n}$	(TS01)	EuF_n^{+3-n}	(HSS95)
AlF_n^{+3-n}	(TS01)	EuO_n^{+3-n}	(HSS95)
$AlH_3SiO_4^{+2}$	(TS01)	EuO_2H (aq)	(HSS95)
$AlSO_4^+$	(TS01)	$EuOH^{+2}$	(HSS95)
Ba^{+2}	(SH88)	$EuSO_4^+$	(HSS95)
$BaCO_3$ (aq)	(SSH97)	F^-	(SH88)
$BaCl^+$	(SSH97)	$Fe(OH)_4^-$	(DSM99)
BaF^+	(SSH97)	Fe^{+2}	(SSW97)
$BaOH^+$	(SSW97)	Fe^{+3}	(SSW97)
CO_2 (aq)	(SHS89)	$FeCl^+$	(SSH97)
CO_3^{-2}	(SH88)	$FeCl^{+2}$	(SSH97)
Ca^{+2}	(SH88)	$FeCl_2$ (aq)	(SSH97)
$Ca(HCO_3)^+$	(AZ99)	FeF^+	(SSH97)
$CaCO_3$ (aq)	(SSH97)	FeF^{+2}	(SSH97)
$CaCl_n^{+2-n}$	(SSH97)	FeO (aq)	(SSW97)
CaF^+	(SSH97)	$FeOH^+$	(SSW97)
$CaOH^+$	(AZ99)	$FeOH^{+2}$	(SSW97)
$CaSO_4$ (aq)	(SSH97)	Gd^{+3}	(SH88)
Ce^{+3}	(SSW97)	$Gd(CO_3)^+$	(HSS95)
$Ce(CO_3)^+$	(HSS95)	$Gd(HCO_3)^{+2}$	(HSS95)
$Ce(HCO_3)^{+2}$	(HSS95)	$GdCl_n^{+3-n}$	(HSS95)
$CeCl_n^{+3-n}$	(HSS95)	GdF_n^{+3-n}	(HSS95)
CeF_n^{+3-n}	(HSS95)	GdO_n^{+3-n}	(HSS95)
CeO_n^{+3-n}	(HSS95)	GdO_2H (aq)	(HSS95)
CeO_2H (aq)	(HSS95)	$GdOH^{+2}$	(HSS95)
$CeOH^{+2}$	(HSS95)	$GdSO_4^+$	(HSS95)
$CeSO_4^+$	(HSS95)	H^+	(SH88)
Cl^-	(SH88)	H_2 (aq)	(SHS89)
Dy^{+3}	(SH88)	$HAlO_2$ (aq)	(SSW97)
$Dy(CO_3)^+$	(HSS95)	HCO_3^-	(SH88)
$Dy(HCO_3)^{+2}$	(HSS95)	HCl (aq)	(TZA97)
$DyCl_n^{+3-n}$	(HSS95)	HF (aq)	(SHS89)
DyF_n^{+3-n}	(HSS95)	HF_2^-	(SH88)
DyO_n^{+3-n}	(HSS95)	$HFeO_2^-$	(SSW97)
DyO_2H (aq)	(HSS95)	HO_2^-	(SSW97)
$DyOH^{+2}$	(HSS95)	HSO_4^-	(SH88)
$DySO_4^+$	(HSS95)	$HSiO_3^-$	(SSH97)
Er^{+3}	(SH88)	Ho^{+3}	(SH88)
$Er(CO_3)^+$	(HSS95)	$Ho(CO_3)^+$	(HSS95)
$Er(HCO_3)^{+2}$	(HSS95)	$Ho(HCO_3)^{+2}$	(HSS95)
$ErCl_n^{+3-n}$	(HSS95)	$HoCl_n^{+3-n}$	(HSS95)
ErF_n^{+3-n}	(HSS95)	HoF_n^{+3-n}	(HSS95)
ErO_n^{+3-n}	(HSS95)	HoO_n^{+3-n}	(HSS95)
ErO_2H (aq)	(HSS95)	HoO_2H (aq)	(HSS95)
$ErOH^{+2}$	(HSS95)	$HoOH^{+2}$	(HSS95)
$ErSO_4^+$	(HSS95)	$HoSO_4^+$	(HSS95)
Eu^{+2}	(SSW97)	H_2S (aq)	(SHS89)
Eu^{+3}	(SH88)	HS^-	(SH88)
$Eu(CO_3)^+$	(HSS95)	K^+	(SH88)
$Eu(HCO_3)^{+2}$	(HSS95)	KCl (aq)	(SSH97)
$EuCl_n^{+2-n}$	(HSS95)	$KHSO_4$ (aq)	(SSH97)

KOH (aq)	(SSW97)
KSO_4^-	(SSW97)
La^{+3}	(SH88)
$La(CO_3)^+$	(HSS95)
$La(HCO_3)^{+2}$	(HSS95)
$LaCl_n^{+3-n}$	(HSS95)
LaF_n^{+3-n}	(HSS95)
LaO_n^{+3-n}	(HSS95)
LaO_2H (aq)	(HSS95)
$LaOH^{+2}$	(HSS95)
$LaSO_4^+$	(HSS95)
Lu^{+3}	(SH88)
$Lu(CO_3)^+$	(HSS95)
$Lu(HCO_3)^{+2}$	(HSS95)
$LuCl_n^{+3-n}$	(HSS95)
LuF_n^{+3-n}	(HSS95)
LuO_n^{+3-n}	(HSS95)
LuO_2H (aq)	(HSS95)
$LuOH^{+2}$	(HSS95)
$LuSO_4^+$	(HSS95)
$Mg(HCO_3)^+$	(SK95)
Mg^{+2}	(SH88)
$MgCO_3$ (aq)	(SSH97)
$MgCl^+$	(SSH97)
MgF^+	(SSH97)
$MgOH^+$	(SSW97)
$MgSO_4$ (aq)	(MS97)
Mn^{+2}	(SSW97)
$MnCl^+$	(SSH97)
MnF^+	(SSH97)
MnO_4^-	(SSW97)
$MnOH^+$	(SSW97)
$MnSO_4$ (aq)	(SSH97)
Na(For) (aq)	(SK95)
Na^+	(SH88)
$NaAl(OH)_2F_2$ (aq)	(TS01)
$NaAl(OH)_3F$ (aq)	(TS01)
$NaAl(OH)_4$ (aq)	(TS01)
NaCl (aq)	(SSH97)
NaF (aq)	(SSH97)
$NaHSiO_3$ (aq)	(SSH97)
NaOH (aq)	(SSW97)
$NaSO_4^-$	(PSS95)
Nd^{+3}	(SH88)
$Nd(CO_3)^+$	(HSS95)
$Nd(HCO_3)^{+2}$	(HSS95)
$NdCl_n^{+3-n}$	(HSS95)
NdF_n^{+3-n}	(HSS95)
NdO_n^{+3-n}	(HSS95)
NdO_2H (aq)	(HSS95)
$NdOH^{+2}$	(HSS95)
$NdSO_4^+$	(HSS95)
O_2 (aq)	(SHS89)
OH^-	(SH88)
Pr^{+3}	(SSW97)
$Pr(CO_3)^+$	(HSS95)
$Pr(HCO_3)^{+2}$	(HSS95)
$PrCl_n^{+3-n}$	(HSS95)
PrF_n^{+3-n}	(HSS95)
PrO_n^{+3-n}	(HSS95)
PrO_2H (aq)	(HSS95)
$PrOH^{+2}$	(HSS95)
$PrSO_4^+$	(HSS95)
SiF_6^{-2}	(SH88)
SiO_2 (aq)	(SHS89)
Sm^{+3}	(SH88)
$Sm(CO_3)^+$	(HSS95)
$Sm(HCO_3)^{+2}$	(HSS95)
$SmCl_n^{+3-n}$	(HSS95)
SmF_n^{+3-n}	(HSS95)
SmO_n^{+3-n}	(HSS95)
SmO_2H (aq)	(HSS95)
$SmOH^{+2}$	(HSS95)
$SmSO_4^+$	(HSS95)
SO_4^{-2}	(SH88)
SO_2 (aq)	(SHS89)
Tb^{+3}	(SSW97)
$Tb(CO_3)^+$	(HSS95)
$Tb(HCO_3)^{+2}$	(HSS95)
$TbCl_n^{+3-n}$	(HSS95)
TbF_n^{+3-n}	(HSS95)
TbO_n^{+3-n}	(HSS95)
TbO_2H (aq)	(HSS95)
$TbOH^{+2}$	(HSS95)
$TbSO_4^+$	(HSS95)
Tm^{+3}	(SH88)
$Tm(CO_3)^+$	(HSS95)
$Tm(HCO_3)^{+2}$	(HSS95)
$TmCl_n^{+3-n}$	(HSS95)
TmF_n^{+3-n}	(HSS95)
TmO_n^{+3-n}	(HSS95)
TmO_2H (aq)	(HSS95)
$TmOH^{+2}$	(HSS95)
$TmSO_4^+$	(HSS95)
Yb^{+3}	(SH88)
$Yb(CO_3)^+$	(HSS95)
$Yb(HCO_3)^{+2}$	(HSS95)
$YbCl_n^{+3-n}$	(HSS95)
YbF_n^{+3-n}	(HSS95)
YbO_n^{+3-n}	(HSS95)
YbO_2H (aq)	(HSS95)
$YbOH^{+2}$	(HSS95)
$YbSO_4^+$	(HSS95)

References

Akinfiev N. and Zotov A. (1999) Thermodynamic description of equilibria in mixed fluids (H_2O-non-polar gas) over a wide range of temperature (25-700 °C) and pressure (1-5000 bars). *Geochimica et Cosmochimica Acta* 63, 2025-2041.

Bethke C. M. (1996) *Geochemical Reaction Modeling*. Oxford University Press.

Diakonov I. I., Schott J., Martin F., Harrichourry J.-C., and Escalier J. (1999) Iron(III) solubility and speciation in aqueous solutions. experimental study and modelling: part 1. hematite solubility from 60 to 300°C in NaOH-NaCl solutions and thermodynamic properties of $Fe(OH)_4^-$(aq). *Geochimica et Cosmochimica Acta* 63(15), 2247-2261.

Gammons C. H., Wood S. A., and Williams-Jones A. E. (1996) The aqueous geochemistry of the rare-earth elements and yttrium: VI. Stability of neodymium chloride complexes from 25 to 300 °C. *Geochimica et Cosmochimica Acta* 60(23), 4615.

Gimeno Serrano M. J., Auque Sanz L. F., and Nordstrom D. K. (2000) REE speciation in low-temperature acidic waters and the competitive effects of aluminum. *Chemical Geology* 165(3-4), 167-180.

Haas J. R., Shock E. L., and Sassani D. C. (1995) Rare earth elements in hydrothermal systems: Estimates of standard partial molal thermodynamic properties of aqueous complexes of the rare earth elements at high pressures and temperatures. *Geochimica et Cosmochimica Acta* 59(21), 4329-4350.

Helgeson H. C. (1969) Thermodynamics of hydrothermal systems at elevated temperatures and pressures. *American Journal of Science* 267, 729-804.

Johnson J. W., Oelkers E. H., and Helgeson H. C. (1992) SUPCRT92: a software package for calculating the standard molal thermodynamic properties of minerals, gases, aqueous species and reactions from 1 to 5000 bar, and 0 to 1000 °C. *Computers and Geosciences* 18(7), 899-947.

McCollom T. M. and Shock E. L. (1997) Geochemical constraints on chemolithoautotrophic metabolism by microorganisms in seafloor hydrothermal systems. *Geochimica et Cosmochimica Acta* 61(4375-4391).

Migdisov A. A., Reukov V. V., and Williams-Jones A. E. (2006) A spectrophotometric study of neodymium (III) complexation in sulfate solutions at elevated temperature. *Geochimica et Cosmochimica Acta* 70, 983-992.

Migdisov A. A. and Williams-Jones A. E. (2006) A spectrophotometric study of erbium (III) speciation in chloride solutions at elevated temperatures. *Chemical Geology* 234, 17-27.

Migdisov A. A. and Williams-Jones A. E. (2007) An experimental study of the solubility and speciation of NdF_3 in F-bearing aqueous solutions. *Geochimica et Cosmochimica Acta* 71, 3056-3069.

Migdisov A. A. and Williams-Jones A. E. (2008) A spectrophotometric study of Nd(III), Sm(III) and Er(III) complexation in sulfate-bearing solutions at elevated temperatures. *Geochimica et Cosmochimica Acta* 72, 5291-5303.

Migdisov A. A., Williams-Jones A. E., Normand C., and Wood S. A. (2008) A spectrophotometric study of samarium (III) speciation in chloride solutions at elevated temperatures. *Geochimica et Cosmochimica Acta* 72, 1611-1625.

Migdisov A. A., Williams-Jones A. E., and Wagner T. (2009) An experimental study of the solubility and speciation of the Rare Earth Elements (III) in fluoride- and chloride-bearing aqueous solutions at temperatures up to 300 °C. *Geochimica et Cosmochimica Acta* 73, 7087-7109.

Pokrovski G. S., Schott J., and Sergeyev A. S. (1995) Experimental determination of the stability constants of NaSO4- and NaB (OH)40 in hydrothermal solutions using a new high-temperature sodium-selective glass electrode -- Implications for boron isotopic fractionation. *Chemical Geology* 124(3-4), 253-265.

Shock E. L. and Helgeson H. C. (1988) Calculation of the thermodynamic and transport properties of aqueous species at high pressures and temperatures: Correlation algorithms for ionic species and equation of state predictions to 5 kb and 1000°C. *Geochimica et Cosmochimica Acta* 52(8), 2009-2036.

Shock E. L., Helgeson H. C., and Sverjensky D. A. (1989) Calculation of the thermodynamic and transport properties of aqueous species at high pressures and temperatures: Standard partial molal properties of inorganic neutral species. *Geochimica et Cosmochimica Acta* 53(9), 2157-2183.

Shock E. L. and Koretsky C. M. (1995) Metal-organic complexes in geochemical processes: Estimation of standard partial molal thermodynamic properties of aqueous complexes between metal cations and monovalent organic acid ligands at high pressures and temperatures. *Geochimica et Cosmochimica Acta* 59(8), 1497-1532.

Shock E. L., Sassani D. C., Willis M., and Sverjensky D. A. (1997) Inorganic species in geologic fluids: Correlations among standard molal thermodynamic properties of aqueous ions and hydroxide complexes. *Geochimica et Cosmochimica Acta* 61(5), 907-950.

Sverjensky D. A., Shock E. L., and Helgeson H. C. (1997) Prediction of the thermodynamic properties of aqueous metal complexes to 1000°C and 5 kb. *Geochimica et Cosmochimica Acta* 61(7), 1359-1412.

Tagirov B. and Schott J. (2001) Aluminum speciation in crustal fluids revisited. *Geochimica et Cosmochimica Acta* 65(21), 3965-3992.

Tagirov B. R., Zotov A. V., and Akinfiev N. N. (1997) Experimental study of dissociation of HCl from 350 to 500°C and from 500 to 2500 bars: Thermodynamic properties of HCl°(aq). *Geochimica et Cosmochimica Acta* 61(20), 4267-4280.

Wagman D. D., Evans W. H., Parker V. B., Schumm R. H., Halow I., Bailey S. M., Churney K. L., and Nuttall R. L. (1982) The NBS tables of chemical thermodynamic properties: Selected values for inorganic and C_1 and C_2 organic substances in SI units. *Journal of Physical Chemistry Reference Data* 11, supplement no. 2, 392 p.

Wolery T. J. and Jarek R. L. (2003) *Software User's Manual EQ3/6, Version 8.0*. Sandia National Laboratories - U.S. Department of Energy Report, Albuquerque, NM.

Wood S. A., Palmer D. A., Wesolowski D. J., and Bénézeth P. (2002) The aqueous geochemistry of the rare earth elements and yttrium: Part XI. The solubility of $Nd(OH)_3$ and hydrolysis of Nd^{3+} from 30 to 290 °C at saturated water vapor pressure with in-situ pH_m measurement. In *Water-Rock Interaction, Ore Deposits and Environmental Geochemistry: A Tribute to David A. Crerar. The Geochemical Society Special Publication*, Vol. 7 (ed. R. Hellmann and S. A. Wood), pp. 229-256.